Short title: IRT1-dependent Fe partitioning into shoots

Title:

Root-to-shoot iron partitioning in Arabidopsis requires IRON-REGULATED TRANSPORTER1 (IRT1)

Author names and affiliations:

Julia Quintana[1], María I. Bernal[1,2], Marleen Scholle[1], Heike Holländer-Czytko[1], Nguyen Nga[3], Markus Piotrowski[1], David G. Mendoza-Cózatl[3], Michael J. Haydon[1,4], Ute Krämer[1,§]

[1]Faculty of Biology and Biotechnology, Ruhr University Bochum, 44801 Bochum, Germany

[2]Department of Plant Nutrition, Estación Experimental de Aula Dei-CSIC, 50059 Zaragoza, Spain

[3]Division of Plant Sciences, MU-Columbia, Columbia, MO 65211-7310, USA

[4]Present address: School of BioSciences, University of Melbourne, Melbourne, Australia

[§]**Corresponding author**: Ute.Kraemer@ruhr-uni-bochum.de

Professor Dr. Ute Krämer

Ruhr University Bochum

Chair of Molecular Genetics and Physiology of Plants

Universitätsstraße 150, Box 44, ND3/30

D-44801 Bochum, Germany

Tel.: +49 (0)234 32 24291; FAX: +49 (0)234 32 14187

One sentence summary: The Arabidopsis high-affinity root Fe^{2+} uptake system IRT1 is also required for Fe partitioning from the root to the shoot.

List of author contributions: M.J.H., M.B. and U.K. conceived the project, M.J.H., M.B., J.Q. and U.K. designed research, J.Q., M.B., M.J.H., M.S., H.H.-C. and M.P. performed experiments, J.Q., M.B., M.J.H. and U.K. analyzed data, N. N. and D. M.-C. confirmed independently short-term Fe uptake, J.Q. and U.K. wrote the manuscript, with contributions from M.B., M.J.H. and H.H.-C. All authors read and edited the manuscript.

Funding information: This work was supported by Deutsche Forschungsgemeinschaft grants Kr1967/3-3 and 15-1, European Union FOOD-CT-2006-016253 and ERC-AdG LEAP EXTREME (788380) to U.K., Ruhr University Bochum (U.K.), European Union fellowship PIIF-GA-2008-219457 to M.J.H., Araid-Ibercaja-young scientist grant 2010 (M.B), as well as Juan de la Cierva (MICINN) and JAE-DOC (CSIC) (M.B.).

ABSTRACT

IRON-REGULATED TRANSPORTER1 (IRT1) is the root high-affinity ferrous iron uptake system and indispensable for the completion of the life cycle of *Arabidopsis thaliana* without vigorous iron (Fe) supplementation. Here we provide evidence supporting a second role of IRT1 in root-to-shoot mobilization of Fe. We show that the *irt1*-2 (*pam42*) mutant over-accumulates Fe in roots, most prominently in the cortex of the differentiation zone, when compared to the wild type. Shoots of *irt1*-2 are severely Fe-deficient according to Fe content and marker transcripts, as expected. We generated *irt1*-2 lines producing IRT1 mutant variants carrying single amino-acid substitutions of key residues in transmembrane helices IV and V, Ser_{206} and His_{232}, which are required for transport activity in yeast. In the transgenic Arabidopsis lines, short-term root Fe uptake rates and secondary substrate Mn accumulation resemble those of *irt1*-2, suggesting that these plants remain incapable of IRT1-mediated root Fe uptake. Yet, $IRT1_{S206A}$ partially complements rosette dwarfing and leaf chlorosis, as well as root-to-shoot Fe partitioning and gene expression defects of *irt1*-2, all of which are fully complemented by wild-type IRT1. Taken together, these results suggest a function for IRT1 in root-to-shoot Fe partitioning that does not require Fe transport activity of IRT1. Among the genes of which transcript levels are partially dependent on IRT1, we identify *MYB DOMAIN PROTEIN10*, *MYB DOMAIN PROTEIN72* and *NICOTIANAMINE SYNTHASE4* as candidates for effecting IRT1-dependent Fe mobilization in roots. Understanding the biological functions of IRT1 will help to improve iron nutrition and the nutritional quality of agricultural crops.

52 **INTRODUCTION**

53 The evolution of core components of electron transport chains and central metabolic pathways
54 predated the Great Oxidation Event, which was accompanied by a dramatic decrease in the
55 bioavailability of iron (Fe) approximately 2 Ga ago (Alberts et al., 2002). In all living organisms, the
56 nutritional requirement for the micronutrient Fe is thus generally far higher than bioavailable
57 concentrations in today's biosphere. Fe is the third most limiting mineral nutrient in agriculture (Zuo
58 and Zhang, 2011), and one-third of the World's population suffer from Fe-deficiency anemia (Lopez
59 et al., 2016). As primary producers, land plants possess particularly effective mechanisms for mining
60 Fe from the Earth's crust, and bio-available Fe in plant biomass contributes to sustaining ecosystems
61 and human nutrition.

62 IRON REGULATED TRANSPORTER1 (IRT1) is the *bona fide* high-affinity root Fe^{2+} uptake system
63 and of central importance in plants pursuing strategy I of iron acquisition, including *Arabidopsis*
64 *thaliana* (Henriques et al., 2002; Varotto et al., 2002; Vert et al., 2002; Eide et al., 1996; Connolly et
65 al., 2002; Kobayashi and Nishizawa, 2012). Arabidopsis *irt1* mutants have severely chlorotic leaves,
66 are strongly impaired in growth and die before reaching the reproductive stage unless supplemented
67 with Fe chelates. The IRT1 protein forms a complex with the FERRIC REDUCTION OXIDASE2
68 (FRO2) and AUTOINHIBITED PLASMA MEMBRANE H^+-ATPase2 (AHA2) for $Fe^{(+III)}$
69 solubilization and Fe^{2+} uptake into epidermal cells in the root differentiation zone (Martín-Barranco et
70 al., 2020). Besides IRT1, the high-affinity Mn transporter NATURAL RESISTANCE-ASSOCIATED
71 MACROPHAGE PROTEIN1 (NRAMP1) is thought to act as a secondary low-affinity Fe^{2+} uptake
72 system (Cailliatte et al., 2010; Castaings et al., 2016).

73 In Fe-deficient plants, increased transcription of *IRT1*, *FRO2* and *AHA2* is thought to be controlled by
74 the basic HELIX-LOOP-HELIX (bHLH) transcription factor FE-DEFICIENCY INDUCED
75 TRANSCRIPTION FACTOR (FIT, bHLH29) (Colangelo and Guerinot, 2004; Jakoby et al., 2004;
76 Bauer et al., 2007; Schwarz and Bauer, 2020). UPSTREAM REGULATOR of IRT1 (URI)/bHLH121,
77 in turn, mediates the transcriptional activation of *FIT* under Fe deficiency (Gao et al., 2019a; Kim et
78 al., 2019; Gao et al., 2020b; Lei et al., 2020). Low Fe availability induces URI phosphorylation, which
79 activates the formation heterodimers of URI with bHLH34/104 or bHLH115 (ILR3) (Kim et al., 2019;
80 Gao et al., 2020a). These heterodimers then bind to the promoters of several Fe deficiency-activated
81 regulators of Fe homeostasis in roots such as the *MYB DOMAIN PROTEIN10* (*MYB10*)/*MYB*
82 *DOMAIN PROTEIN72* (*MYB72*) and *bHLH38/39/100/101*. Notably, the interaction of transcription
83 factors bHLH38/39/100/101 with FIT is necessary for the FIT-dependent activation of *IRT1, FRO2*
84 and *AHA2* (Wang et al., 2007; Sivitz et al., 2012). When a physiologically sufficient level of Fe is
85 restored, FIT is polyubiquitinated by BRUTUS-LIKE1/2 (BTSL1/2) and targeted for degradation in
86 the vacuole (Sivitz et al., 2011; Rodríguez-Celma et al., 2019).

87 IRT1 appears to undergo continuous cycling between the endosomal compartment and the plasma
88 membrane where IRT1 is active (Barberon et al., 2011; Barberon et al., 2014; Ivanov et al., 2014). The

89 monoubiquitination of IRT1 triggers its trafficking from the plasma membrane to the early endosome,
90 which can constitute the first step towards the degradation of IRT1 in the vacuole (Kerkeb et al., 2008;
91 Barberon et al., 2011). Monoubiquitination, internalization and degradation of IRT1 are strongly
92 impaired in synthetic IRT1 variants carrying mutations of both lysine residues K154 and K179 in the
93 cytosolic loop between transmembrane helices III and IV (Kerkeb et al., 2008; Barberon et al., 2011).
94 SORTING NEXIN1 (SNX1) in the early endosome and the phosphatidylinositol-3-phosphate binding
95 protein FYVE-DOMAIN PROTEIN1 (FYVE1) in the late endosome contribute to the cellular sorting
96 of IRT1, including its delivery to the plasma membrane that counteracts the degradation of
97 endocytosed IRT1 protein (Barberon et al., 2014; Ivanov et al., 2014).
98 IRT1 lacks specificity for its primary substrate Fe^{2+}, so that it can inadvertently transport other cations
99 present in the soil solution such as Mn^{2+}, Cd^{2+}, Zn^{2+} and Co^{2+} (Eide et al., 1996; Rogers et al., 2000;
100 Vert et al., 2002; Connolly et al., 2002). For example, IRT1 was concluded to be the major route for
101 the intake of non-essential hazardous Cd^{2+} cations into Arabidopsis and likely also into many food
102 crops (Vert et al., 2002). To counteract the accumulation of toxic metals under Fe deficiency,
103 excessive cytosolic levels of secondary-substrate metal cations are sensed by binding to a histidine-
104 rich sequence motif in the cytosolic loop located between the transmembrane domains III and IV of
105 IRT1 (Dubeaux et al., 2018). This leads to the phosphorylation of serine and threonine residues in the
106 same cytosolic loop of IRT1 by CBL-INTERACTING PROTEIN KINASE23 (CIPK23), thus
107 triggering the extension of monoubiquitination into K63-polyubiquitination mediated by IRT1
108 DEGRADATION FACTOR1 (IDF1), followed by the vacuolar degradation of IRT1 (Dubeaux et al.,
109 2018; Shin et al., 2013). FRO2 and AHA2 can also be ubiquitinated, but – different from IRT1 – their
110 post-translational modification is independent of non-target secondary IRT1 substrate metal cations
111 (Martín-Barranco et al., 2020).
112 Besides its localization at the root surface for Fe^{2+} cation uptake by the plant, IRT1 was also detected
113 in the root vasculature (Barberon et al., 2011; Marquès-Bueno et al., 2016). Only the combined
114 expression of *IRT1* in both, trichoblasts and phloem companion cells, complemented the dwarfed
115 growth, leaf chlorosis, and infertility of the *irt1* mutant cultivated in soil (Marquès-Bueno et al., 2016).
116 Moreover, the *IRT1* mRNA was reported to move from the shoot into the root, suggesting its cell-to-
117 cell mobility (Thieme et al., 2015). The function of *IRT1* expression in phloem companion cells has
118 remained elusive to date.
119 Here we provide evidence for a secondary role of IRT1 in root-to-shoot Fe partitioning, independent
120 of its transmembrane Fe^{2+} transport activity. Our results show an over-accumulation of Fe in roots of
121 the *irt1* mutant, whereas *irt1* shoots are severely Fe-deficient in comparison to wild type plants. We
122 then transformed the *irt1* mutant with *IRT1* constructs encoding transport-inactive mutant protein
123 variants $IRT1_{S206A}$ and $IRT1_{H232A}$. Short-term root Fe uptake rates and accumulation of the secondary
124 IRT1 substrate Mn are indistinguishable from *irt1* in these lines, as expected. Nevertheless, $IRT1_{S206A}$
125 partially rescues rosette dwarfing and leaf chlorosis, as well as alterations in root-to-shoot Fe

126 mobilization and Fe status marker transcript levels, of *irt1*. Using transcriptomics, we further identify
127 *MYB10*, *MYB72* and their target of transcriptional activation *NICOTIANAMINE SYNTHASE4 (NAS4)*
128 as candidates for downstream involvement in IRT1-dependent root-to-shoot Fe partitioning, among
129 other genes.
130
131

132 **RESULTS**

133 **Root-to-shoot iron partitioning is altered in the *irt1* mutant**

134 To examine how Fe concentrations are altered in roots and shoots of the *irt1* mutant, we compared
135 wild-type (WT) and *irt1*-2 seedlings (*pam42*, termed *irt1* below). Seedlings were cultivated under Fe-
136 deficient (- Fe, no added Fe) and Fe-sufficient (+ Fe, 10 µM FeHBED, control) conditions for 10 d,
137 subsequent to a 10-d pre-cultivation period on Fe-sufficient standard medium (Fig. 1A). Upon
138 cultivation in control conditions, shoot Fe concentrations were about one-third lower in *irt1* seedlings
139 than in the WT (Fig. 1B). On Fe-deficient media, Fe concentrations were equivalent in shoots of *irt1*
140 and WT, a known consequence of growth limitation by Fe deficiency (Fig. 1B, Supplemental Fig. S1A
141 and B) (Baxter et al., 2008). In roots, Fe concentrations were about twice as high in *irt1* than in the
142 WT when cultivated under control conditions (Fig. 1C). A similar trend was observed upon cultivation
143 in Fe-deficient media, but the difference between *irt1* and WT was not statistically significant (Fig.
144 1C). Thus, shoot Fe concentrations were in agreement with expectations, but root Fe concentrations
145 were contrary to expectations, based on the role of IRT1 as the primary root Fe uptake system of
146 Arabidopsis. Congruent with these observations, root-to-shoot Fe concentration ratios were invariably
147 close to unity in WT, but they were strongly shifted towards root Fe accumulation in *irt1* on both
148 control and Fe-deficient media (Fig. 1D). Accounting for condition- and genotype-dependent
149 differences in the degree of Fe limitation of growth (Supplemental Fig. S1A and S1B), total Fe
150 contents (Supplemental Fig. S1C and D) were also in agreement. Taken together, these results suggest
151 a substantial reduction in the partitioning of Fe from roots to shoots in *irt1* mutant plants, in addition
152 to their previously described well-known iron uptake defect (Henriques et al., 2002; Vert et al., 2002).
153 In order to address where over-accumulation of Fe occurs in the roots of *irt1* seedlings, we performed
154 histochemical detection of non-heme $Fe^{(+II,\ +III)}$ in roots after desorbing apoplastically bound Fe. We
155 confirmed that roots of the constitutively iron-deficient *frd3-7* mutant over-accumulate Fe in the stele,
156 as previously reported (Green and Rogers, 2004). Whole-mount Perls staining of roots of seedlings
157 grown on standard media was in agreement with elevated Fe levels in *irt1* compared to the WT, in
158 which we did not observe any insoluble precipitates of Prussian blue (Fig. 2). In *irt1* roots, the Perls
159 stain was localized in the two sub-epidermal cell layers of the differentiation zone, most prominently
160 in the cortex, and not visible in the stele, different from the *frd3-7* mutant. This observation is
161 consistent with impaired Fe movement into the stele of *irt1*, and it cannot be explained by the loss of
162 the cellular Fe import function of IRT1, which is primarily localized in root epidermal cells (Vert et
163 al., 2002; Marquès-Bueno et al., 2016).

164

165 **$IRT1_{S206A}$ variant partially complements the *irt1* mutant**

166 AtIRT1 unequivocally functions in plant Fe uptake by transporting Fe^{2+} cations across the plasma
167 membrane of root epidermal cells (Vert et al., 2002). To test for any additional, distinct role of IRT1 in
168 Fe homeostasis, we used site-directed mutagenesis to construct variants of *IRT1* (Supplemental Fig.

Figure 1

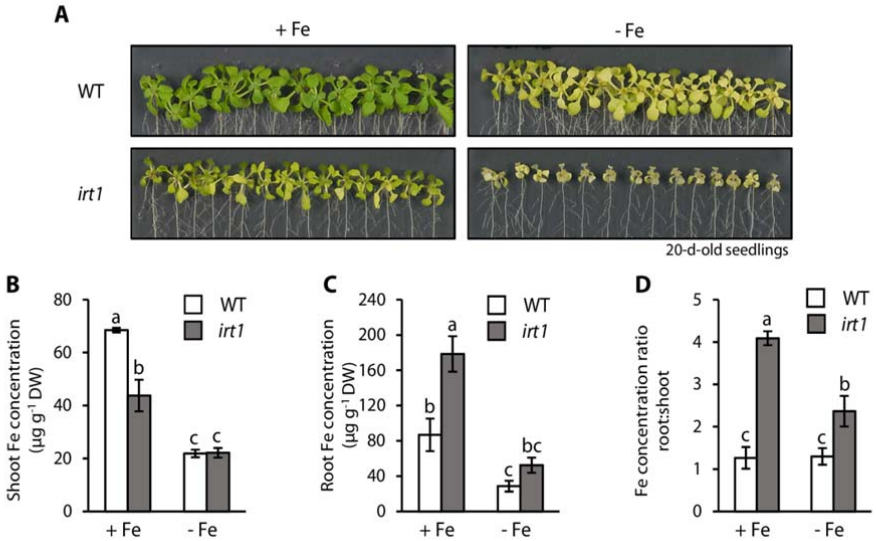

Figure 1. The irt1 mutant overaccumulates Fe in the root whereas the shoot is Fe-limited. (A) Photographs of 20-d-old WT and irt1 seedlings grown in Fe-sufficient (+ Fe, 10 ı M FeHBED) and Fe-deficient (- Fe, 0 ı M FeHBED) agar-solidified 0.25x modified Hoagland˘s medium (EDTA-washed agar) for 10 d, subsequent to an initial cultivation in standard medium (5 ı M FeHBED, unwashed agar) for 10 d, on vertically oriented petri plates. (B - D) Shoot (B) and root (C) Fe concentrations and root:shoot Fe concentration ratio (D) in 20-d-old WT and irt1 seedlings. Seedlings were grown as in (A). Bars represent arithmetic mean ě SD (n = 3 pools of tissue, each from 15 (WT) or 30 (irt1) seedlings, with 15 seedlings cultivated per plate). Distinct letters indicate statistically significant differences (P < 0.05, two-way ANOVA followed by Tukeyús HSD test). Data show one experiment representative of three independent experiments. DW: dry biomass.

169 S2) that encode $IRT1_{S206A}$ (serine at position 206 substituted by alanine) and $IRT1_{H232A}$ (histidine at
170 position 232 substituted by alanine). Previous work had shown that both of these IRT1 mutant variants

Figure 2

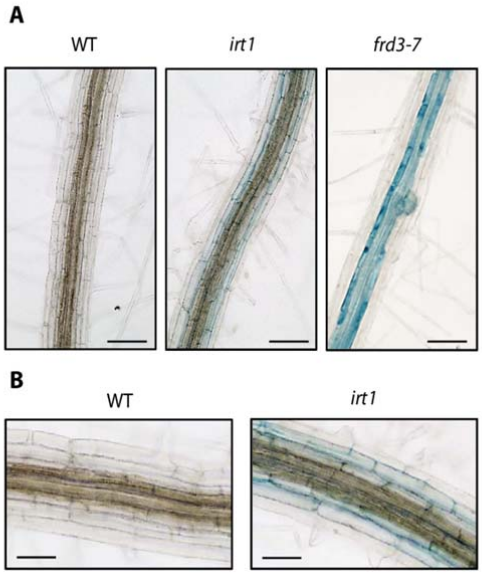

Figure 2. Fe accumulates in sub-epidermal cell layers of irt1 roots. (A) Histochemical detection of labile $Fe^{(+II, +III)}$ by Perls stain in the root differentiation zone of 7-d-old WT, irt1 and frd3-7 seedlings grown on agar-solidified 0.25x modified Hoagland˘s medium (5 ı M FeHBED). (B) Magnified image (20x) of WT and irt1 roots shown in (A). Photographs are representative of n = 10 to 12 roots from two independent experiments, each with seedlings cultivated on three replicate petri plates processed in parallel. Scale bars: 100 ı m (A), 50 ı m (B).

171 were unable to transport both Fe^{2+} and non-target substrates Zn^{2+}, Mn^{2+} and Cd^{2+} in the heterologous
172 yeast system *Saccharomyces cerevisiae* (Rogers et al., 2000). Genomic sequences corresponding to

173 the coding region of *IRT1* variants and WT *IRT1* were placed downstream of the native *IRT1* promoter
174 (1,024 bp) and upstream of the native genomic *IRT1* terminator (310 bp). We obtained Arabidopsis
175 *irt1* $IRT1_P$:$IRT1_{S206A}$ (termed *irt1* S206A) and *irt1* $IRT1_P$:$IRT1_{H232A}$ (*irt1* H232A) lines capable of
176 producing transport-inactive IRT1 only, as well as complemented lines *irt1* $IRT1_P$:*IRT1* (*irt1* IRT1;
177 Supplemental Table S1). *IRT1* transcripts were at comparable levels in the WT and the two
178 complemented lines, and undetectable in the *irt1* mutant (Supplemental Fig. S3A). For both *irt1*
179 S206A and *irt1* H232A, *IRT1* transcript levels were comparable to the WT in one line and
180 approximately tripled those of the WT in the other line, in - Fe-grown seedlings. By comparison, in +
181 Fe-grown seedlings of all genotypes *IRT1* transcript levels were down to a small fraction of between
182 5% and 16%, except in the *irt1* H232A lines, in which transcript levels in + Fe remained at between
183 64% and 89% of those in - Fe. Note that in our transgenic *irt1* lines, *IRT1* transcript levels are
184 influenced by both the genomic environment of the T-DNA and the physiological Fe status of
185 seedlings, some of which possess only a transport-inactive IRT1 protein. In contrast to *IRT1*, maximal
186 *IRT2* transcript levels remained below WT levels in all lines and were less than 6.5% of those of *IRT1*
187 in iron-deficient WT seedlings (Supplemental Fig. S3A). Thus, it appears that the T-DNA insertion in
188 *irt1*-2 (*pam42*) within the transcribed region 96 bp upstream of the translational start codon of *IRT1*
189 and about 2,700 bp downstream of the last exon of *IRT2*, also disrupted the function of *IRT2* (Varotto
190 et al., 2002).
191 IRT1 protein abundance in roots largely reflected *IRT1* transcript levels (Fig. 3A, see Supplemental
192 Fig. S3A). IRT1 protein levels were comparable to the wild type in *irt1* S206A line 2, and elevated
193 compared to both the complemented lines and the wild type in line 1 (Fig. 3A, Supplemental Fig.
194 S3B). Importantly, IRT1 protein was detectable in roots of WT seedlings cultivated on our Fe-
195 sufficient control media, supporting a role of IRT1 in Fe acquisition also under these cultivation
196 conditions (Supplemental Fig. S3B).
197 In the two *irt1* S206A lines, seedling growth and rosette color, leaf chlorophyll concentrations and
198 root growth all suggested a partial complementation of *irt1* mutant phenotypes by comparison to the
199 WT and *irt1*/IRT1 complemented lines (Fig. 3B-D). By contrast, the *irt1* H232A lines resembled the
200 *irt1* mutant throughout. Similarly, soil-grown vegetative *irt1* S206A plants were of a similar size and
201 green color as the WT and *irt1* *IRT1* complemented lines, whereas *irt1* H232A lines were
202 indistinguishable from the *irt1* mutant (Supplemental Fig. S4). Rosettes of *irt1* S206A line 2 appeared
203 to be slightly larger and greener than those of line 1 (Fig. 3B, Supplemental Fig. S4). The partial
204 complementation of the *irt1* mutant phenotype through the $IRT1_{S206A}$ variant of an amino acid residue
205 required for transport activity is in agreement with our hypothesis of a secondary biological function
206 of IRT1 in addition to transmembrane Fe^{2+} transport. The $IRT1_{H232A}$ variant of IRT1 was unable to
207 complement the *irt1* mutant phenotype, consistent with a model in which H232 is indispensable for
208 both Fe transport and any additional role in Fe homeostasis carried out by IRT1.

Figure 3

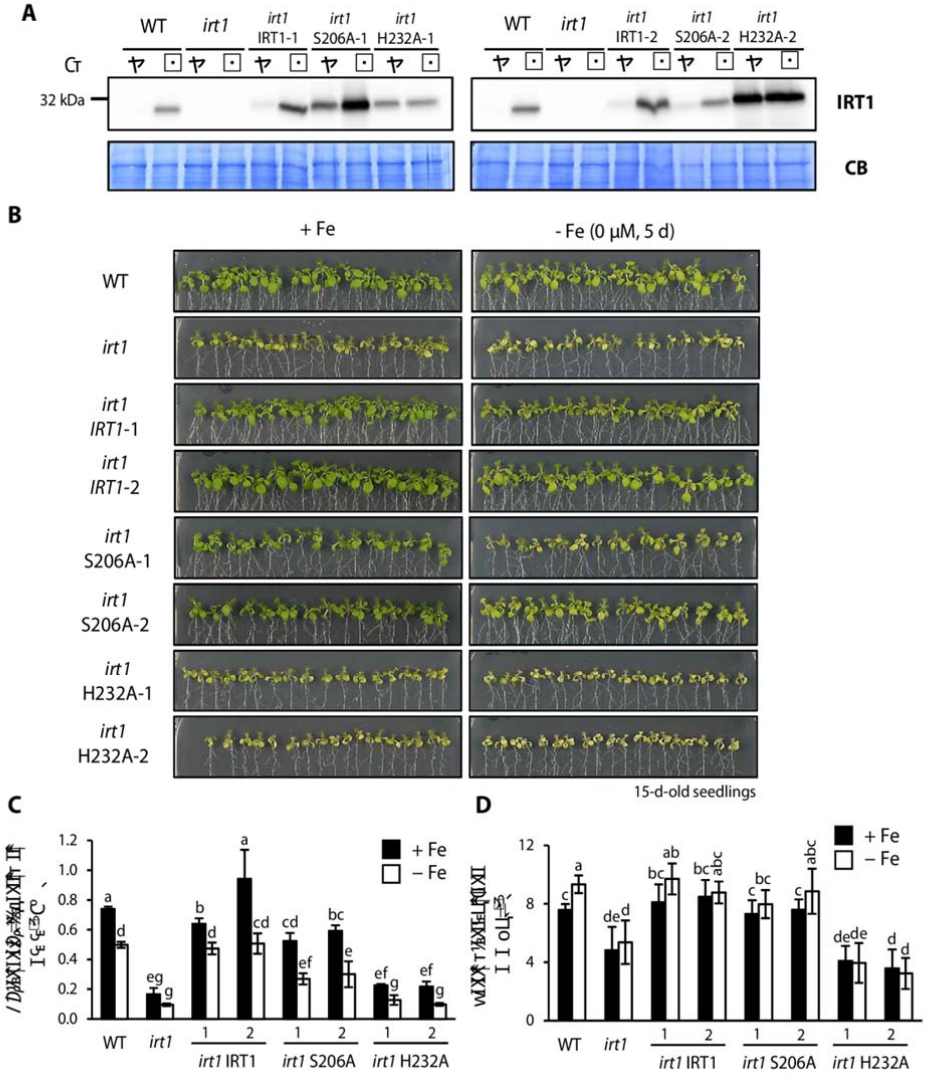

Figure 3. Fe transport-inactive $IRT1_{S206A}$ partially complements irt1. (A - D) Immunoblot detection of IRT1 protein (A), photographs (B), leaf chlorophyll concentrations (C) and mean root elongation over the last 5 d of growth (D) in 15-d-old seedlings of WT, irt1, irt1 IRT1, irt1 S206A and irt1 H232A. Seedlings were grown on Fe-sufficient (+ Fe, 10 ı M FeHBED) and Fe-deficient (- Fe, 0 ı M FeHBED) agar-solidified 0.25x modified Hoagland˘s medium (EDTA-washed agar) for 5 d, subsequent to an initial cultivation period of 10 d in standard medium (5 ı M Fe-HBED; unwashed agar), on vertically oriented petri plates. Total root protein extracts (20 ≈g) were separated on denaturing gels and blotted onto PVDF membranes, with the Commassie Blue-stained (CB) PVDF membrane shown as loading control (A). Bars represent arithmetic mean ě SD (n = 4 pools of 5 to 8 shoots (C); n = 8 to 10 roots (D)). Distinct letters indicate significant differences (P < 0.05) according to two-sample Student˘s or Welch t-tests upon correction for multiple comparisons (C) or two-way ANOVA followed by Tukeyús HSD test (D). Images in (A) are representative of three replicate membranes. Data are from two independent experiments, each with two (C) or one (D) replicate plates.

209 Next we sought to confirm that the *irt1* S206A and *irt1* H232A mutants cannot transport Fe^{2+}. In
210 contrast to the WT IRT1 protein, both $IRT1_{S206A}$ and $IRT1_{H232A}$ failed to complement the growth

Figure 4

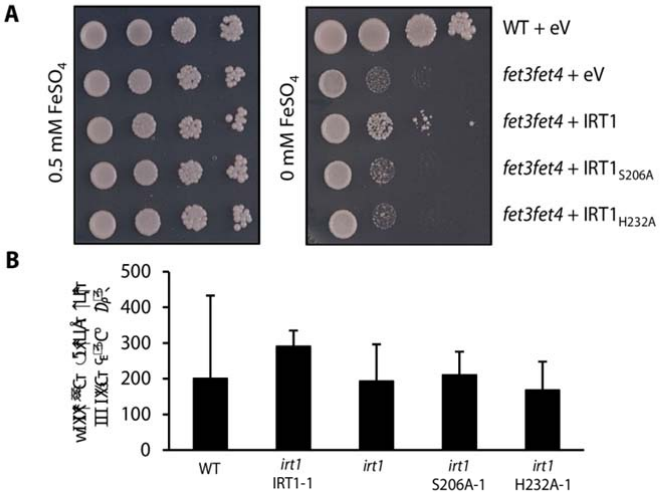

Figure 4. Yeast complementation assay and root $^{55}Fe^{2+}$ uptake rates. (A) Growth of WT and the fet3fet4 Fe transport-defective mutant transformed with a modified pFL61 plasmid as empty vector (eV), or containing the IRT1, $IRT1_{S206A}$ or $IRT1_{H232A}$ cDNA, respectively. Ten-fold serial dilutions of liquid cultures were spotted on SD (-Ura) medium (pH 5.7) supplemented with 0.5 mM $FeSO_4$ or left unamended. (B) Uptake rates determined in hydroponically cultivated 7.5 to 8.5-w-old plants over a 13.5-min period. Before the initiation of uptake assays, plants were exposed to Fe deficiency (0 ı M FeHBED) for 6 d, subsequent to an initial cultivation period in 1x modified Hoagland:s solution containing 10 mM FeHBED (WT and irt1 IRT1) or 50 mM FeHBED (all other genotypes) for 6 to 7 weeks. Bars represent arithmetic mean ě SD (n = 4 to 5 plants). Data show one experiment representative of three independent experiments (see Supplemental Table S2).

211 impairment of an iron uptake-defective *S. cerevisiae fet3fet4* mutant on low-iron media (Fig. 4A), as
212 reported previously (Rogers et al., 2000). In order to obtain *in planta* evidence, we quantified $^{55}Fe^{2+}$

213 incorporation into roots of *ca*. 8-week-old hydroponically cultivated WT, *irt1*, *irt1* IRT1, *irt1* S206A
214 and *irt1* H232A plants after exposure to Fe deficiency for a period of 6 d. Short-term uptake rates of
215 $^{55}Fe^{2+}$ into roots were not decreased in *irt1* by comparison to the WT (Figure 4B, Supplemental Table
216 S2). This result was contrary to expectations, given the lack of the high-affinity root Fe^{2+} uptake
217 system in the *irt1* mutant, and it precluded the complementation testing that we had intended to
218 achieve with this experiment. Importantly, we also detected no differences in root $^{55}Fe^{2+}$ uptake rates
219 between *irt1* S206A and *irt1* H232A, indicating against the differential activation of any secondary Fe
220 uptake systems as the cause for their differing phenotypes (Figure 4B). Altogether, these results
221 suggest that roots of mutants lacking IRT1 transport activity retain significant root Fe^{2+} uptake rates
222 under the employed conditions, which is counter-intuitive but consistent with previously published
223 results including one short-term and one longer-term radiotracer uptake experiment (Henriques et al.,
224 2002; Vert et al., 2002).
225
226 **The root-to-shoot Fe partitioning defect of *irt1* is partially rescued by the transport-inactive**
227 **$IRT1_{S206A}$ variant**
228 We observed root Fe over-accumulation in *irt1*, as well as a partial complementation of growth
229 impairment and chlorosis of *irt1* by a transport-inactive $IRT1_{S206A}$ mutant (see Figs. 1C, 2 and 3). Next
230 we addressed root-to-shoot Fe partitioning. Shoot Fe concentrations were significantly higher in *irt1*
231 S206A lines compared to *irt1* following growth in control media, and indistinguishable from *irt1* in
232 *irt1* H232A (Fig. 5A and B). Note that all three of these genotypes are physiologically Fe-deficient in
233 control media because they share the lack of IRT1-mediated high-affinity root Fe uptake. Upon
234 growth on Fe-deficient media, there was little or no difference in shoot Fe concentrations between WT
235 and *irt1* (as noted before, see Fig. 1), indicating that this condition is generally less informative
236 (Figure 5A and B). Fe allocation to shoots corroborated a partial complementation in *irt1* S206A lines
237 of the root-to-shoot Fe partitioning defect of *irt1* (Fig. 5C and D). Shoot Mn concentrations were in
238 agreement with the lack of active IRT1 protein in the roots, because the levels of Mn – as a secondary
239 substrate of IRT1 – were similar in shoots of the *irt1* mutant and the transport-inactive lines (Fig. 5E
240 and F).
241 Root Fe accumulation of *irt1* mutants was restored down to levels resembling the WT in *irt1* S206A
242 seedlings, but not in *irt1* H232A, under control conditions (Supplemental Fig. S5A and B). Note that
243 *irt1 IRT1* lines contained higher *IRT1* transcript and IRT1 protein levels than the WT under + Fe
244 conditions (see Supplemental Fig. S3B), which affects Fe homeostasis, and that *irt1* H232A seedlings
245 of line 2 were very small and chlorotic (see Fig. 3). Total Fe per plant in the *irt1* H232A lines was
246 similar to (*irt1* H232A-1), or even lower (*irt1* H232A-2) than, total Fe in the *irt1* mutant. In *irt1* S206
247 lines, total Fe was consistently higher than total Fe of *irt1* and the *irt1* H232A lines, and lower than, or
248 similar to, WT and *irt1* IRT1, in control conditions (Supplemental Fig. S5C and D). We propose that
249 increased total Fe levels in the *irt1* S206A lines could be attributed to larger seedling size, a larger root

Figure 5

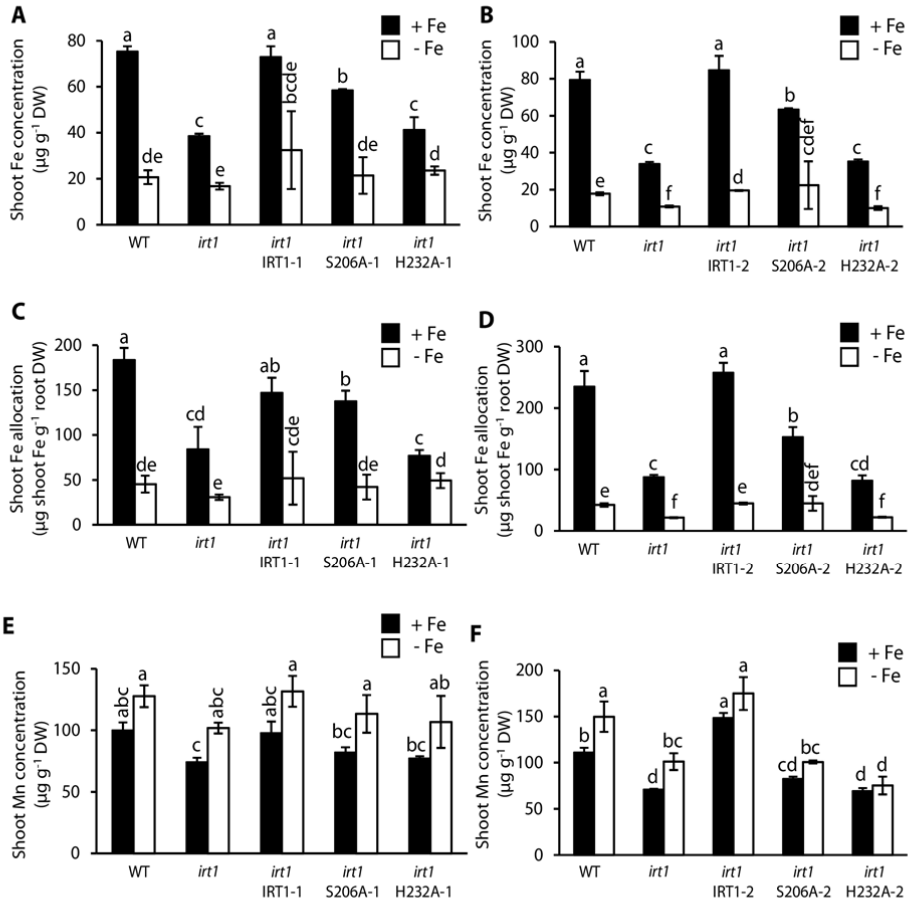

Figure 5. Partial rescue of root-to-shoot Fe allocation in irt1 S206A. (A - F) Shoot Fe concentration (A and B), shoot Fe allocation (C and D) and shoot Mn concentrations (E and F) in 20-d-old seedlings of WT, irt1, irt1 IRT1, irt1 S206A and irt1 H232A grown on Fe-sufficient (+ Fe, 10 ı M FeHBED) and Fe-deficient (- Fe, 0 ı M FeHBED) agar-solidified 0.25x modified Hoagland˘s medium (EDTA-washed agar) for 10 d, subsequent to an initial cultivation period of 10 d in standard medium (5 ı M FeHBED; unwashed agar), on vertically oriented petri plates. Bars represent arithmetic mean ě SD (n = 3 pools of tissues, each from 15 to 30 seedlings, with 15 seedlings cultivated per plate). Distinct letters indicate significant differences (P < 0.05) according to two-sample Student˘s t-tests upon correction for multiple comparisons (A - D) or in two-way ANOVA followed by Tukeyús HSD test (E and F). Data show one experiment representative of two independent experiments.

surface area resulting from a longer root in *irt1* S206A than in *irt1* (see Fig. 3), or differing overall Fe homeostasis as a consequence of altered Fe distribution within the plant. In *irt1*, *irt1* S206A and *irt1*

252 H232A, root concentrations of the secondary IRT1 substrate Mn were generally far lower than in both
253 WT and *irt1* IRT1 seedlings, in which they increased under - Fe with increasing IRT1 protein levels,
254 as expected (see Supplemental Fig. S3). Root *NRAMP1* transcript levels were 2 to 3.3-fold elevated in
255 *irt1* and *irt1 H232A* lines, when compared to the WT (Supplemental Fig. S5G). In *irt1* S206A they
256 were lower and remained only slightly, between 1.3- and 1.8-fold, increased compared to *NRAMP1*
257 transcript levels of the WT and *irt1* IRT1 lines. These observations are consistent with IRT1 being the
258 predominant membrane transport protein contributing to root Mn levels under our experimental
259 conditions. In *irt1* S206A-1, root Mn concentrations approximated WT levels under + Fe, although
260 remaining below these on average. The fact that root Mn concentrations did not increase at all on - Fe
261 medium in the presence of increased levels of $IRT1_{S206A}$ protein (see Supplemental Fig. S3) suggested
262 against a direct causal involvement of $IRT1_{S206A}$. Taking these results together, residual IRT1 transport
263 activity or an activation of a secondary Fe uptake system, including *NRAMP1*, cannot explain the
264 partial complementation of shoot Fe levels in *irt1* S206A lines (see Fig. 5A and B). In summary, the
265 root-to-shoot iron partitioning defect of the *irt1* mutant is partially rescued by the transport-inactive
266 $IRT1_{S206A}$, but not $IRT1_{H232A}$.
267 Ferritins are plastid-localized iron storage proteins, and their levels increase when plants are Fe-replete
268 (Briat et al., 2009). In shoots of WT and *irt1* IRT1 seedlings cultivated on - Fe media for 5 d,
269 *FERRITIN1* (*FER1*) transcript levels were as low as 4.6 to 6.7% of those observed in control media
270 (Fig. 6A). *FER1* expression in *irt1* H232A under control conditions was comparable to that of *irt1* and
271 Fe-deficient WT (Fig. 6A). *FER1* transcript levels in shoots of *irt1* S206A lines were intermediate
272 between WT and *irt1*, in agreement with growth and Fe contents in these lines (Fig. 6A, compare Fig.
273 5 and Fig. S5). In roots, the differences in *FER1* transcript levels between lines were qualitatively
274 similar, but quantitatively much smaller, in line with root Fe levels (Fig. 6B. compare Fig. 5 and
275 Supplemental Fig. S5). Transcript levels of Fe deficiency marker genes *IRONMAN1* (*IMA1)*, *ZINC*
276 *INDCED FACILITATOR1* (*ZIF1*), *bHLH39* and *NAS4* in shoots further corroborated a partial
277 complementation of *irt1* by $IRT1_{S206A}$, as evident upon cultivation in control media (Supplemental Fig.
278 S6).
279
280 **How is Fe homeostasis altered in roots of *irt1*?**
281 Next we examined whether Fe status marker genes can additionally provide insights into Fe
282 homeostasis in the *irt1* mutant and thus into possible secondary functions of the IRT1 protein.
283 According to all the marker genes analyzed, the degree of physiological Fe deficiency in shoots of the
284 *irt1* mutant grown in control media was approximately equivalent to, or slightly more severe, than in
285 the WT after 5 d of cultivation on Fe-deficient media (Fig. 6, Supplemental Fig. S6). Note that we
286 quantified biomass and mineral contents of tissues after 10-d treatments in order to avoid experimental
287 noise from low biomass of some samples and the associated sensitivity of our results to contamination,
288 for example from dust particles. Considering roots, *FER1* transcript levels in Fe-deficient WT and *irt1*

Figure 6

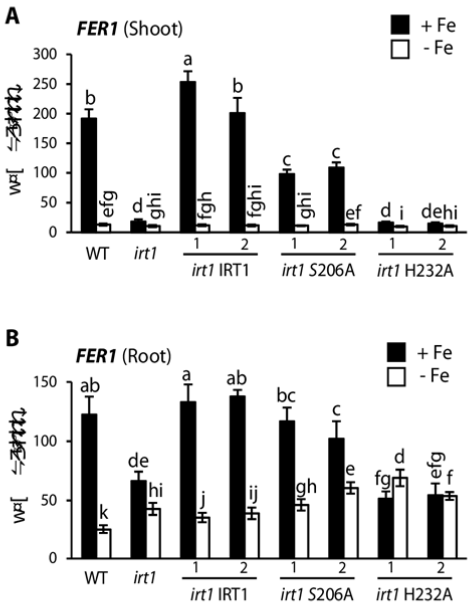

Figure 6. FER1 transcript levels. (A - C) Relative transcript levels (RTL) of FER1 in shoots (A) and roots (B) of 15-d-old WT, irt1, irt1 IRT1, irt1 S206A, irt1 H232A seedlings. RTL are shown normalized to both UBQ10 and EF1*a* as constitutively expressed control genes. Seedlings were grown on Fe-sufficient (+ Fe, 10 ı M FeHBED) and Fe-deficient (- Fe, 0 ı M FeHBED) agar-solidified 0.25x modified Hoagland˘s medium (EDTA-washed agar) for 5 d, subsequent to an initial cultivation period of 10 d in standard medium (5 ı M FeHBED; unwashed agar), on vertically oriented petri plates. Bars represent arithmetic mean ě SD (n = 6 technical replicates on cDNA obtained using tissue pooled from 2 to 3 plates, each with 20 seedlings). Distinct letters indicate significant differences (P < 0.05) according to two-sample Student˘s or Welch t-tests upon correction for multiple comparisons. Data show one experiment representative of three independent experiments.

289 IRT1 seedlings were 20 to 28% of those observed in Fe-replete media (Fig. 6B). When compared to
290 the WT, *FER1* transcript levels in roots of the *irt1* mutant were reduced to a clearly lesser extent than

291 in shoots after cultivation under control conditions. However, root *FER1* transcript levels did not fully
292 reflect increased root Fe concentrations in *irt1* compared to the WT (compare Fig. 6B with Figs. 1C,
293 2A). *FER1* transcript levels are highly localized according to the eFP browser in 7-day-old seedlings,
294 with at least 3.5 times higher *FER1* transcript levels in root endodermal and phloem companion cells
295 and at least 2.5 times higher *FER1* transcript levels in root pericycle cells than in root cortex and
296 epidermal cells (Supplemental Fig. S9A) (Brady et al., 2007; Winter et al., 2007). All in all, these
297 results suggest a more Fe-replete status in roots than in shoots of *irt1*, supporting that root-
298 accumulated Fe is at least partly physiologically accessible and thus intracellular in the *irt1* mutant.
299
300 **Additional genes of the root Fe-deficiency response are mis-regulated in *irt1***
301 Next we addressed transcriptome differences between *irt1* and the WT in order to identify candidate
302 genes for mediating decreased root-to-shoot iron mobility in the *irt1* mutant. Between 3 and 5 d of Fe
303 deficiency were previously shown to result in maximal transcriptional responses in roots (Connolly et
304 al., 2002; Connolly et al., 2003; Vert et al., 2003). In our experimental conditions, root surface Ferric
305 Chelate Reductase (FCR) activity in WT seedlings reached a maximum at 5 days of Fe deficiency
306 (Supplemental Fig. S7A). At the time point selected for harvest, FCR activity of the *irt1* mutant was
307 3.2-fold higher than that of WT under control conditions (+ Fe; Supplemental Fig. S7B). In the WT,
308 FCR activity was 6.6-fold higher under - Fe than under + Fe conditions, and approximately 2-fold
309 higher than in the *irt1* cultivated on + Fe medium (Supplemental Figure S7B).
310 We conducted microarray-based transcriptomics in 15-day-old WT and *irt1* seedlings grown in Fe-
311 replete media (+ Fe) as well as WT seedlings cultivated in Fe-deficient (- Fe) media for the final 5 d
312 before harvest (see also previous section). A comparison between - Fe and + Fe conditions in WT
313 seedlings identified the transcriptomic Fe deficiency response under our experimental conditions (- Fe
314 *vs.* C (WT)). The comparison between *irt1* and WT cultivated under + Fe conditions identified all
315 symptoms and consequences of the lack of IRT1 (*irt1 vs.* WT (C)). Finally, we compared between *irt1*
316 cultivated under + Fe conditions and WT cultivated under - Fe conditions to identify transcriptome
317 aberrations in the *irt1* mutant (*irt1* (C) *vs.* WT - Fe) (Supplemental Fig. S7C).
318 In our transcriptomics attempt to identify candidate genes for altered root-to-shoot Fe partitioning in
319 the *irt1* mutant, we expected that candidate gene transcript levels respond to Fe deficiency because
320 IRT1 protein levels also respond to iron deficiency. *IRT1* is expressed in roots, and roots are the
321 primary organ that governs root-to-shoot translocation of mineral nutrients. Among the transcripts of
322 which levels increased more than 2-fold under - Fe compared to control conditions in WT roots, 44%
323 had higher levels in *irt1* than WT under control conditions (Figure 7A, - Fe *vs*. C (WT) ↑ AND *irt1 vs*.
324 WT (C) ↑). Approximately three quarters of these transcripts increased in abundance in *irt1* similarly
325 to the increase in Fe-deficient WT (Supplemental Dataset S2). But for the remaining 26% of these
326 transcripts, this increase was clearly less pronounced than expected from the physiological Fe status of
327 *irt1* plants (Fig. 7A, *irt1 vs*. WT (- Fe) ↓, marked by a single asterisk; see above). This group of 20

Figure 7

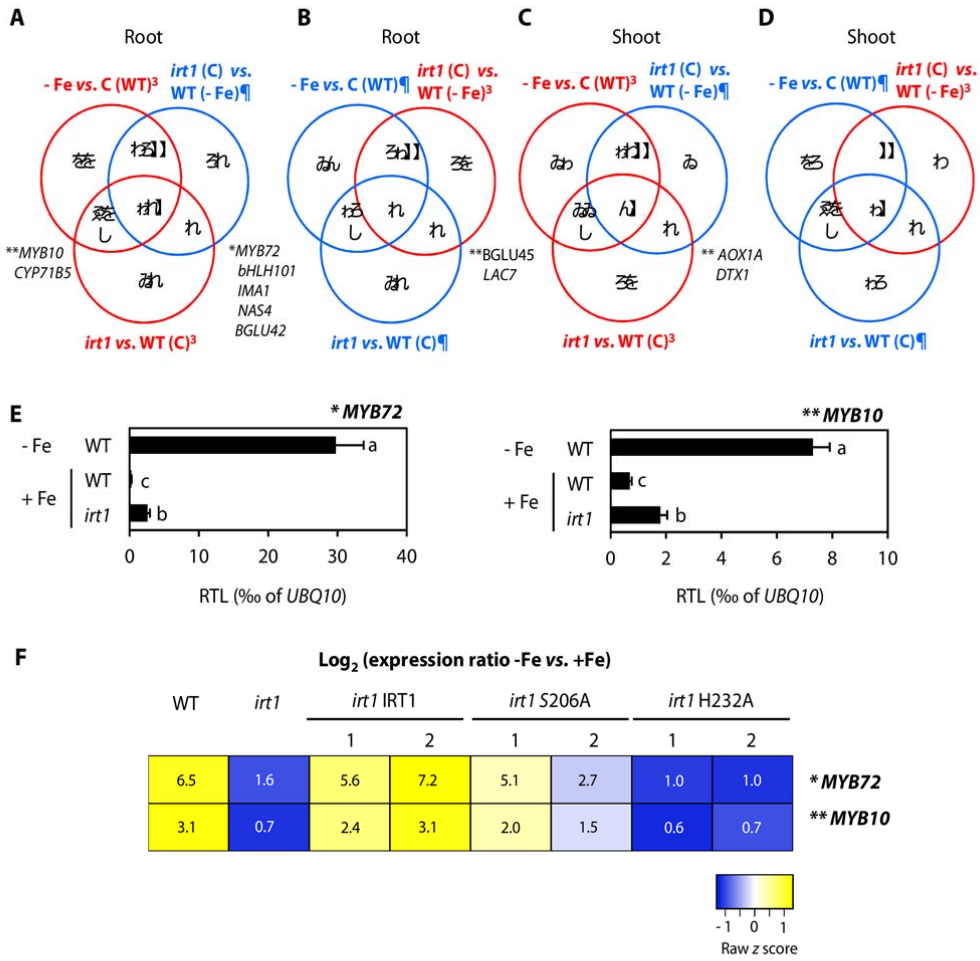

Figure 7. Transcriptome analysis of irt1 compared to Fe-deficient and -sufficient WT seedlings. (A - D) Summary of microarray-based transcriptome data in roots (A and B) and shoots (C and D). Shown within Venn diagrams are the numbers of genes with ħ 2-fold differences in transcript levels in different comparisons (P < 0.15). Colors denote responses, (red/blue, higher/lower transcript abundance in one genotype and/or condition compared to the other). Symbols denote Fe deficiency-responsive transcripts that are deregulated (*, **) or not (#) in irt1. (E) Relative transcript levels (RTL) of MYB10 and MYB72 in roots of WT and irt1 seedlings. RTL are shown normalized to UBQ10. (F) Heat map of MYB72 and MYB10 transcript abundance - Fe vs. + Fe in roots of different genotypes as indicated. Numbers are Log_2 (transcript level ratios, with RTL normalized to both UBQ10 and EF1*a*), and raw z-score for each gene was used to scale the heat map, from three independent experiments. WT and irt1 seedlings were grown on Fe-sufficient (+ Fe, 10 ı M FeHBED) and Fe-deficient (- Fe, 0 ı M FeHBED) agar-solidified modified 0.25x Hoagland˘s medium (EDTA-washed agar) for 5 d, subsequent to an initial cultivation period of 10 d in standard medium (5 ı M FeHBED; unwashed agar), on vertically oriented petri plates (A - F). Bars represent arithmetic mean ě SD (n = 3 technical replicates on cDNA obtained using tissue pooled from 2 to 3 plates, each with 20 seedlings (E)). Distinct letters indicate significant differences (P < 0.05) in two-way ANOVA followed by Tukeyús HSD test (MYB10) or two-sample Student˘s t-tests upon correction for multiple comparisons (MYB72). Data in (F) are from three independent experiments.

genes comprises candidates for an IRT1-dependent function in root-to-shoot partitioning of Fe. The corresponding genes included a number of functionally uncharacterized or poorly characterized genes,

330 as well as previously characterized Fe homeostasis genes including *MYB72*, *IMA1, bHLH101*, *NAS4*
331 and *BETA-GLUCOSIDASE42* (*BGLU42*), for example (Supplemental Dataset S1; note that *bHLH100*
332 and *bHLH38*, which are similar to *bHLH101* in both sequence and biological function, are not
333 represented on the microarray). Of the transcripts that decreased in abundance under - Fe *vs*. C (WT)
334 and also in *irt1 vs*. WT (C), none were under-responsive in *irt1* (Fig. 7B, asterisk).
335 A severe de-regulation in the *irt1* mutant was apparent for a total of 43 Fe deficiency-responsive
336 transcripts of WT, which were not significantly regulated in the same direction in *irt1 v*s. WT (C), and
337 thus showed an unexpected non-responsiveness in *irt1*. These more promising candidate genes for an
338 IRT1-dependent function in root-to-shoot Fe partitioning included *MYB10* and *CYTOCHROME P450*
339 *71B5* (*CYP71B5*) (up in WT -Fe) as well as *BETA-GLUCOSIDASE45* (*BGLU45*) and *LACCASE7*
340 (*LAC7*) (down in WT -Fe), for example (Fig. 7A and B, double asterisks; Supplemental Dataset S1).
341 Transcript levels of *MYB10* and *CYP71B5* are known to respond strongly to Fe deficiency (Buckhout
342 et al., 2009; Yang et al., 2010). *BGLU45* and *LAC7* are thought to function in cell wall lignification
343 (Chapelle et al., 2012; Schulten and Krämer, 2017).
344 We cannot exclude that causative genes may act in shoots, given that *IRT1* expression in phloem
345 companion cells was reported to be critical for its *in planta* function (Marquès-Bueno et al., 2016).
346 In shoots, 76% and 71% of the transcripts that differed in abundance in *irt1* compared to WT under
347 control conditions were also up- or down-regulated, respectively, when WT was exposed to Fe
348 deficiency (Figure 7C, *irt1 vs.* WT (C) ↑ AND - Fe *vs.* C (WT) ↑; Supplemental Dataset S4). Again,
349 some of those transcripts were not up- or down-regulated as expected in Fe-deficient *irt1*, e.g.
350 *ALTERNATIVE OXIDASE1* (*AOX1A*) or *DETOXIFICATION1* (*DTX1*) (Figure 7C and D, double
351 asterisks; Supplemental Dataset S3).
352 In an independently cultivated experiment, compared to + Fe, the levels of the root-specific transcript
353 *MYB72* were up-regulated *ca.* 100-fold in -Fe-grown WT, but in *irt1* they reached only about 8% of
354 the transcript levels in -Fe-grown WT according to RT-qPCR, thus fully confirming the microarray
355 data (Figure 7E). For *MYB10*, a 10-fold increase in transcript levels was observed in the WT in - Fe,
356 whereas increase in *irt1* was only about 2.6-fold (Fig. 7E, compare with 3-fold change, not statistically
357 significant, according to the microarrays). The *CYP71B5* expression profile was similar to that of
358 *MYB10* and *MYB72* (Supplemental Fig. S8A and E). Thus, according to RT-qPCR, *MYB10* and
359 *CYP71B5* also form part of the regulatory category represented by *MYB72*, so that the microarrays
360 may have been insufficiently sensitive to detect this (Fig. 7A, *). RT-qPCR also suggested that the
361 *bHLH39* expression ratio between *irt1* and -Fe-grown WT was 2.7, whereas the microarray data had
362 suggested a ratio below 2 (Fig. 7A, #; Supplemental Fig. S8B and E). Both microarray and RT-qPCR
363 results supported that root transcript levels of *CYP71B5* were severely under-responsive, and those of
364 *bHLH39* were considerably more responsive, to the general Fe deficiency in *irt1* seedlings. In shoots,
365 fully confirming the microarray data, RT-qPCR detected no statistically significant difference in
366 transcript levels of *NAS4* between WT - Fe and *irt1* + Fe (Supplemental Fig. S8D and E). Transcript

367 levels of *DTX1*, however, in *irt1* were only about 16% of those in WT - Fe (Supplemental Fig. S8C
368 and E), also confirming the microarray data. Thus, in shoots of *irt1*, *DTX1* transcript levels did not
369 follow the physiological Fe status, whereas *NAS4* transcript levels did.
370 Further consideration of these data highlights some complexities affecting the identification of
371 candidate genes for a role in IRT1-dependent root-to-shoot Fe partitioning. Importantly, the de-
372 regulation of expression of Fe deficiency-responsive genes in the *irt1* mutant could well constitute the
373 cause of altered Fe partitioning in the *irt1* mutant, congruent with candidate gene status. However, the
374 altered expression of such genes in *irt1* could also merely reflect as a consequence the locally altered
375 physiological status of Fe or even of secondary substrate metals in *irt1* by comparison to the WT or of
376 the dynamics of Fe deficiency responses over time. Complicating this even further, the cell-
377 autonomous, non-cell-autonomous or even systemic contributions of the transcriptional regulation of
378 these genes have not been established yet. Finally, the cell type-specificity of candidate gene
379 expression in relation to Fe localization were not considered in our transcriptomics experiment.
380 To begin to tackle this latter issue, we next attempted to employ information from publicly available
381 cell type-specific gene expression data. Using the GEO2R tool and available cell-type specific datasets
382 (GEO; https://www.ncbi.nlm.nih.gov/geo/, GSE10501), we identified transcripts that are at least 2-
383 fold more abundant either in the cortex or in the endodermis than in the stele under conditions of - Fe
384 (24 h treatment) (Dinneny et al., 2008; Supplemental Figure 9A). Among these genes, we then focused
385 on the subgroup of genes for which our data indicated differential transcript abundance in WT roots
386 between - Fe and + Fe conditions, as putative reporters of local Fe status (Supplemental Dataset S5;
387 Supplemental Dataset S6). However, the expression of many of these genes is likely to be systemically
388 controlled according to the iron status of the shoot, like *IRT1* (Vert et al., 2003). Therefore, among the
389 chosen genes, we finally identified those genes as putative markers of local Fe status, of which
390 transcript levels in *irt1* followed Fe distribution across its roots (See Fig.1B), i.e. did not suggest a
391 more deficient physiological Fe status in *irt1 vs*. WT roots under control conditions. Expression of 38
392 Fe deficiency-responsive genes is higher in the cortex than in the stele, including *BGLU45*, *ZRT/IRT-*
393 *LIKE PROTEIN2* (*ZIP2*)*, NAS1, AT3G43670* and *BTSL2*, for example (Dinneny et al., 2008).
394 Additionally, their transcript levels did not show a statistically significant Fe deficiency response in
395 *irt1* compared to WT under control conditions, according to our microarray data from bulk root tissues
396 (Supplemental Dataset S5). We confirmed this by RT-qPCR for *BGLU45* and *BTSL2* (Supplemental
397 Fig. S9B). Given that published data from promoter-GUS fusions of *BTSL2* (Rodríguez-Celma et al.,
398 2019) rather suggest a broad expression domain in Fe-deficient roots, the most promising marker
399 transcript that may reflect local Fe status in root cortex cells remains *BGLU45* encoding beta-
400 glucosidase 45.
401
402 **Candidate genes for roles in IRT1-dependent root-to-shoot Fe partitioning**

403 We identified a group of Fe deficiency-responsive genes as under-responsive in roots of the *irt1*
404 mutant (Fig. 7, * and **; Supplemental Datasets S1 and S2). Among these, we identified *MYB72* and
405 *MYB10* as candidates for putative roles in IRT1 protein-dependent root-to-shoot Fe translocation, for
406 example. Therefore, we analyzed transcript levels of *MYB72* and *MYB10* across our panel of
407 transgenic lines, following cultivation as for microarray-based transcriptomics. Indeed, roots of *irt1*
408 S206A lines responded to Fe deficiency, compared to control conditions, with a larger increase of
409 *MYB72* and *MYB10* expression than in *irt1* and *irt1* H232A (Fig. 7F; Supplemental Fig. S10).
410 Additional candidate genes that are also Fe status markers, *NAS4* and *IMA1*, exhibited a similar
411 expression pattern (Supplemental Figure S10). These observations can be interpreted as a partial
412 complementation of an attenuated Fe deficiency responsiveness in *irt1* roots (see Fig. 7). Different
413 from *irt1* S206A, changes in transcript levels between Fe deficiency and Fe replete conditions
414 suggested that the response of *irt1* H232A to Fe levels in the media was overall similarly attenuated as
415 in the *irt1* mutant (Fig. 7). Together, these results are consistent with possible roles of the transcription
416 factor-coding genes *MYB72* and *MYB10* as well as their target gene *NAS4*, and *IMA1*, in IRT1-
417 dependent root-to-shoot Fe partitioning, but further work will be required to obtain unequivocal
418 evidence for such a role of these or other candidate genes.
419
420

421 **DISCUSSION**

422 **High root Fe concentrations in the *irt1* mutant**

423 Our results indicate that roots of the *irt1* mutant accumulate Fe (Fig. 1; Supplemental Fig. S5). By
424 contrast, shoots of the *irt1* mutant – as is well established and confirmed again here – contain reduced
425 Fe concentrations as long as Fe is not growth-limiting, compared to the WT (Figs. 1 and 5). Several
426 earlier studies suggested that the *irt1* mutant may contain unexpectedly high levels of Fe in the root,
427 but the physiological significance of this had remained unaddressed (Henriques et al., 2002; Cailliatte
428 et al., 2010; Ivanov et al., 2014). Indeed, the use of EDTA as a chelator of Fe^{3+} in the synthetic media
429 of these studies favored the precipitation of Fe (Chaney, 1988; Becher et al., 2004; Salomé et al.,
430 2014) and consequently the authors very appropriately considered that an incomplete desorption of
431 apoplastically precipitated or bound Fe could have affected their results. In this study, the use of
432 HBED as Fe^{3+} chelator in combination with a comparably low total Fe concentration are better suited
433 for maintaining Fe^{III} in solution in a synthetic medium. In line with this, Fe concentrations in roots
434 remained in the range of those in shoots of the WT (Fig. 1D).

435 Our histochemical detection of Fe in *irt1* roots using Perls stain located Fe accumulation
436 predominantly in the cortex of the differentiation zone (Fig. 2). We observed no Fe signal in cell walls
437 in general. Transcript levels of a number of Fe status marker genes indicated an overall more sufficient
438 Fe status in roots than in shoots of the *irt1* mutant, which can be taken to support that the Fe
439 accumulated in roots of *irt1* is at least partly intracellular and physiologically accessible (Figs. 6 and 7,
440 Supplemental Figs. S6 to S10). Our targeted search identified *BGLU45* as a possible marker transcript
441 of local Fe status in root cortex cells that is in agreement with Fe levels in the *irt1* mutant
442 (Supplemental Fig. S9), which will require dedicated confirmation in the future. The physiological Fe
443 status of the shoots systemically governs the transcriptional activation of a number of Fe deficiency-
444 related genes in the roots (Vert et al., 2003; Giehl et al., 2012; Mendoza-Cózatl et al., 2014; Khan et
445 al., 2018). This complicates the identification of cell type-specific markers of local iron status in roots.
446 In the *nramp1 irt1* double mutant Perls-DAB staining localized Fe in the walls of cortex cells, and the
447 authors attributed this observation to the lack of *NRAMP1* function in the *irt1* genetic background
448 (Castaings et al., 2016). The extensive sample preparation carried out in this study may have removed
449 intracellularly localized Fe or deposited it onto cell walls.

450 When the high-affinity Fe^{2+} transporter IRT1 or the secondary Fe^{2+} transporter NRAMP1 are not
451 present, endodermal suberization is delayed, which was proposed to facilitate the movement of Fe into
452 the stele upon the entry into roots *via* the apoplastic or trans-cellular pathways (Barberon et al., 2016).
453 Despite the decreased suberization and increased permeability of the endodermis for ions in *irt1*, our
454 results support the hypothesis that Fe is immobilized predominantly in the cortex and also in the
455 endodermis of the *irt1* mutant, i.e., partly outward from the endodermis. This is consistent with our
456 hypothesis that the inward transport of Fe^{2+} across the plasma membrane of root epidermal cells is not
457 the only function of the IRT1 protein.

458

459 **Phenotypic rescue of the root-to-shoot Fe partitioning defect of *irt1* by the transport-inactive**
460 **mutant $IRT1_{S206A}$ variant**

461 Based on the results presented here, we hypothesized that the IRT1 protein acts indirectly to de-repress
462 root-to-shoot partitioning of Fe, in addition to its well-known direct membrane transporter function of
463 mediating the uptake of Fe^{2+} into root cells. If our hypothesis is correct, we would expect to observe
464 the partial complementation of *irt1* mutant phenotypes by an IRT1 variant that is incapable of
465 transporting Fe^{2+} but maintains indirect functionality. While the latter is entirely unknown to date, the
466 direct transmembrane ion transport function of IRT1 is very well-studied. Amino acid residues Serine
467 206 and Histidine 232 are both critical for the cellular import of Fe^{2+} (Fig. 4, Supplemental Fig. S2), as
468 well as of secondary substrates Zn^{2+}, Mn^{2+} and likely also Cd^{2+}, conferred by IRT1 in the heterologous
469 system *Saccharomyces cerevisiae* (Eide et al., 1996; Rogers et al., 2000).

470 We introduced wild-type IRT1, $IRT1_{S206A}$ and $IRT1_{H232A}$ into an *irt1* mutant background and then
471 tested for the rescue of various aspects of phenotype of Arabidopsis *irt1* mutants. Our results are in
472 agreement with our hypothesis, and they indicated that $IRT1_{S206A}$ is inactive with respect to the direct
473 function of IRT1, but maintains the indirect function at least partially. By contrast, our results suggest
474 that $IRT1_{H232A}$ is produced and stable *in planta*, but maintains neither the direct nor the indirect
475 function of IRT1. We came to these conclusions by quantifying Fe concentrations and Fe deficiency
476 symptoms in roots and shoots of seedlings (Figs. 3 - 7, Supplemental Figs. S3 to S8). Important
477 support came from the quantification of Mn concentrations in tissues, exploiting the known transport
478 activity of IRT1 for the secondary substrate Mn^{2+} in combination with IRT1 protein abundance under
479 deficient and replete physiological Fe status (Figs. 3 and 5, Supplemental Figs. S3 and S5; Vert et al.,
480 2002).

481 Intriguingly, we were unable to identify any difference between WT and *irt1* roots in short-term Fe
482 accumulation, i.e. after 15 min of exposure to 2 µM radiolabeled Fe^{2+} (Fig. 4B, Supplemental Table
483 S2). Previous evidence from short-term Fe uptake assays *in planta* is scarce. In contrast to 2-w-old Fe-
484 deficient WT plants, the *irt1* mutant (Ws background) was incapable of accumulating ^{55}Fe in shoots
485 after 48 hours (Vert et al., 2002). Wild-type roots contained approximately 50% and *irt1*-3 roots 70%
486 of the total Fe accumulated per plant upon 1 h of pulse-labeling with 3 µM ^{59}Fe-labeled Fe^{2+} *via* the
487 roots of 2-w-old seedlings cultivated in Fe- and Zn-deficient medium. There was large quantitative
488 variation and total Fe uptake averaged of 130 ± 60 and 80 ± 30 fmol Fe $plant^{-1}$ in WT and *irt1*-3,
489 respectively, and images suggested an overall smaller size of *irt1*-3 than of WT seedlings used in the
490 pulse labeling experiments (Henriques et al., 2002; T-DNA insertion 133 bp upstream of translational
491 start codon). Although a direct or quantitative comparison with these two earlier studies is impossible,
492 our results are in general agreement. Taking these studies together, the unequivocal defect in *irt1*
493 mutants is a dramatically reduced Fe accumulation rate in shoots, whereas root Fe accumulation rate in
494 *irt1* is unchanged or even slightly enhanced. Thus, *irt1* mutants retain some root Fe uptake capacity

495 independent of the IRT1 protein, suggesting that secondary Fe uptake systems operate in these
496 mutants under the experimental conditions employed. An involvement of NRAMP1, for example, is
497 possible, as proposed (Cailliatte et al., 2010; Castaings et al., 2016).
498
499 **Candidate genes for a role in IRT1-dependent Fe partitioning from the root to the shoot**
500 Our results support the hypothesis of a secondary function of IRT1 in the partitioning of Fe from the
501 root to the shoot, which is at least partially independent of the primary function of IRT1 in root
502 cellular Fe uptake. Such a secondary function of IRT1 could involve a physical interaction of IRT1
503 with an unknown protein, which then triggers a process that finally results in the radial passage of Fe
504 from root cortex cells inwards, for example. According to a symplastic pathway model, this IRT1-
505 dependent process could encompass maintaining symplastic mobility of Fe through its chelation in the
506 cytosol, suppressing the immobilization of Fe in vacuoles of root cortex cells, or fostering symplastic
507 radial cell-to-cell passage of Fe *via* plasmodesmata. In a transcellular pathway model, the envisaged
508 process could involve cellular Fe efflux from root cortex cells and Fe re-uptake by endodermal cells.
509 Proteins mediating any of these processes in a localized fashion remain unidentified. IRT1-dependent
510 de-repression of root-to-shoot partitioning may occur entirely through translational or post-
511 translational regulation, or it may involve changes in transcript levels of some of the involved genes.
512 Here we searched for candidate Fe deficiency-responsive transcripts that were under-responsive or
513 non-responsive in roots of the *irt1* mutant.
514 By comparison to Fe-deficient WT, in roots of *irt1* we observed lower expression of several FIT-
515 dependent (e.g. *CYP71B5, BGLU42*) and FIT-independent (e.g. *NAS4, bHLH101*) genes, among
516 others (Supplemental Datasets S1 and S3; Colangelo and Guerinot, 2004; Bauer et al., 2007;
517 Zamioudis et al., 2015; Schwarz and Bauer, 2020). Notably, the Fe deficiency-responsive increase in
518 *MYB10* and *MYB72* transcript levels was strongly attenuated in *irt1* (Fig. 7). Root-specific
519 transcription factors MYB72 and MYB10 regulate Fe partitioning to the shoot *via* activating *NAS4*
520 transcription and thus NA biosynthesis in the stele (Palmer et al., 2013). Later, MYB72 was found to
521 also activate the transcription of genes encoding the enzymes F6´H1 and BGLU42 of the coumarin
522 biosynthesis pathway that contribute to Fe mobilization in soil (Schmid et al., 2014; Zamioudis et al.,
523 2014; Stringlis et al., 2018). In summary, candidate genes *MYB72* and *MYB10*, and indirectly *NAS4*,
524 may well account for impaired root-to-shoot partitioning of Fe in *irt1*. However, for these and a
525 number of other potential candidate genes (Supplemental Datasets S1 to S4), we were unable to fully
526 resolve whether their de-regulation is the cause or the effect of Fe immobilization in *irt1* roots.
527
528 **CONCLUSIONS**
529 Here we provide evidence for a secondary function of IRT1 in the partitioning of Fe from the root to
530 the shoot. The ability of a transport-inactive $IRT1_{S206A}$ variant to partially complement the *irt1* mutant
531 supports our hypothesis and indicates that the secondary function of IRT1 is at least partly

532 independent of its primary function of high-affinity Fe uptake into root epidermal cells. We identify
533 previously characterized genes as candidate downstream targets of IRT1-dependent transcriptional
534 regulation, which could contribute to Fe mobilization towards the shoot. Future work will be directed
535 at the signaling and mechanisms of IRT1-dependent Fe partitioning from roots to shoots.
536

537 **MATERIALS AND METHODS**

538 **Plant material and growth conditions.** All plant lines used in the present study are in the Col-0
539 background. WT seeds were obtained from NASC. The *irt1*-2 mutant (*pam42*) was from Varotto et al.
540 (2002). The transgenic lines *irt1* $IRT1_P$*:IRT1* (WT *IRT1*), *irt1* $IRT1_P$*:IRT1S206A* (*irt1* S206A) and *irt1*
541 $IRT1_P$*:IRT1H232A* (*irt1* H232A) were generated herein.
542 For sterile growth, seeds were washed in 70% (v/v) ethanol for 1 min, surface-sterilized with 1.4%
543 (w/v) NaOCl and 0.02% (v/v) Triton X-100 for 10 min and washed five times with ultrapure water
544 (Milli-Q; Merck). Following seed stratification at 4°C for 2 d, seedlings were pre-cultivated on a
545 modified Hoagland's solution containing macro- and micronutrients as used in Haydon et al. (2012),
546 supplemented with 1% (w/v) sucrose and solidified with 0.8% (w/v) agar Type M (Sigma). Ten-d-old
547 seedlings were then transferred using titanium tweezers to modified Hoagland's solution
548 supplemented with 1% (w/v) sucrose in which Fe was omitted from the nutrient solutions (- Fe
549 treatment) or supplied as 10 µM FeHBED (+ Fe treatment). Treatment media were solidified with
550 0.8% (w/v) agar Type M (Sigma) depleted from contaminant metals by EDTA-washing as described
551 in Haydon et al. (2012). Seedlings were grown on vertically oriented square 120-mm polystyrene Petri
552 dishes (Greiner Bio-One) in 11-h light (22°C, 145 µmol m^{-2} s^{-1} white light) and 13-h dark (18°C)
553 cycles (Percival CU-41L4; CLF Climatics). For selection of homozygous transgenic lines carrying a
554 single T-DNA insertion, seeds were grown on 0.5x Murashige & Skoog (MS) medium (Duchefa)
555 supplemented with 1% (w/v) sucrose, 0.8% (w/v) agar and hygromycin (30 µg mL^{-1}). In the T2
556 generation, five to six independent lines per construct were grown on MM media (Haydon and
557 Cobbett, 2007) containing 1% (w/v) sucrose and 0.8% (w/v) agar Type M supplemented with
558 hygromycin (30 µg mL^{-1}) for 10 d and then transferred to treatment media (+ Fe treatment, as
559 described above) for an additional 17 d before harvest (see Supplemental Table S1). For hydroponic
560 plant cultivation for short-term uptake assays of radiolabeled Fe, seeds were surface-sterilized, sown
561 on 0.5x modified Hoagland's solution supplemented with 5 µM FeHBED (WT and *irt1* IRT1) or 10
562 µM FeHBED (*irt1*, *irt1* S206A and *irt1* H232A) and solidified with 0.65% (w/v) Noble agar (Sigma)
563 in 0.7 mL black Eppendorf tubes and stratified at 4°C for 4 d. At the age of 7 d, the bottom third of
564 each tube was cut off and about 60 tubes per line (1 seedling per tube) were transferred to a styrofoam
565 tray floating on 4 L of 0.5x modified Hoagland's solution supplemented with 10 µM FeHBED (WT
566 and *irt1* IRT1) or 50 µM FeHBED (*irt1*, *irt1* S206A and *irt1* H232A) in a box covered with Saran
567 wrap. After 1 week, plants were carefully transferred to smaller boxes (4 plants per box in 420 mL
568 solution, keeping roots separate per plant) containing modified Hoagland's solution supplemented

569 with FeHBED as mentioned above (pre-cultivation). Plants were grown for an additional 5 weeks (WT
570 and *irt1* IRT1) to 6 weeks (*irt1*, *irt1* S206A and *irt1* H232A) with a weekly exchange of solutions to
571 obtain vegetative stage plants of similar sizes. Roots were subsequently washed in 10 µM EDTA for 2
572 min and transferred into modified Hoagland's solution lacking FeHBED for 6 days (Fe deficiency
573 treatment). Plants were grown in 11-h light (20°C, 145 µmol m^{-2} s^{-1} white light) and 13-h dark (18°C)
574 cycles (Percival CU-41L4; CLF Climatics) in a tray that was covered with a transparent cover, which
575 was removed during the final 3 weeks of cultivation. For the confirmation experiment at MU, pre-
576 cultivation was in 5 µM (WT) and 50 µM FeHBED (*irt1*) for 4 to 5 w, and Fe deficiency treatment
577 was in 0 µM (WT) and 5 µM (*irt1*) FeHBED for 5 d. For soil cultivation, seeds were germinated on
578 Minitray soil (Balster Einheitserdewerk, Fröndenberg) after 4 days of stratification at 4°C. Plants were
579 grown under the same environmental conditions as for sterile growth for 3 weeks.
580
581 **Yeast Constructs, Strains, and Growth.** The *IRT1* coding cDNA sequence, including translational
582 start and stop codon, was amplified from the corresponding transgenic plant line by RT-PCR with
583 IRT1-ATG_F 5'-CACCATGGCTTCAAATTCAGCAC-3' and IRT1-cDNA_TAA_R 5'-
584 TTAAGCCCATTTGGCGATAATCG-3', introduced into pENTR-D/TOPO (Invitrogen) and cloned
585 into the yeast expression vector pFL61-Gateway (Desbrosses-Fonrouge et al., 2005) using LR clonase
586 (Invitrogen) according to the manufacturer´s protocol. Mutations S206A and H232A were introduced
587 by a modified QuikChange protocol (Zheng et al., 2004) using KAPAHiFi DNA polymerase
588 (PEQLAB Biotechnology) and the primers AtIRT1_S198A_For 5'-
589 TAGTTCACGCGGTGGTCATTGGATTATC-3', AtIRT1_S198A_Rev 5'-
590 CCACCGCGTGAACTATGATCCCAAG-3', AtIRT1_H224A_For 5'-
591 TGCTTCGCTCAAATGTTCGAAGGCATGGG-3' and AtIRT1_H224A_Rev 5'-
592 CATTTGAGCGAAGCAAAGAGCTGCTATAAGTC3'. All constructs were verified by Sanger
593 sequencing. For complementation assays, competent *S. cerevisiae* yeast cells from WT (DY1457) and
594 *fet3fet4* mutant (DEY1453; Dix et al., 1994) strains were transformed with each construct or the empty
595 vector (Dohmen et al., 1991). As a positive control, the corresponding WT yeast strain was
596 transformed with the empty vector. Transformants were selected on SD media lacking uracil (SD-Ura)
597 pH 5.7, 2% (w/v) Bacto-Agar, with 2% (w/v) D-glucose as a carbon source. For each construct, three
598 independent transformant colonies were grown overnight at 30°C in 2 mL liquid SD-Ura pH 3.5 with
599 2% (w/v) D-glucose supplemented with 10 µM $FeCl_3$, to early stationary phase ($OD_{600} \approx 0.3$, *ca.* 10^7
600 cells ml^{-1}). Yeast cells were then centrifuged at 15,700x*g* for 1 min, washed once in SD-Ura pH 5.7
601 with 2% (w/v) D-glucose to remove residual Fe and subsequently resuspended in the same medium.
602 Aliquots of 10 µL of ten-fold serially diluted cell suspensions (OD_{600} of 0.3, 0.03,…) were spotted
603 onto SD-Ura pH 5.7 containing 2% (w/v) Bacto-Agar and 2% (w/v) D-glucose, supplemented with 0.5
604 mM $FeSO_4$ or left unamended. Plates were incubated at 30°C for 3 days and photographed using a
605 Nikon Digital SLR camera with an AF-S DX Zoom NIKKOR 18-70 mm 1:3,5-4,5G ED-IF objective.

606

607 **Generation of transgenic plants.** For genetic complementation of *irt1* mutant with wild-type *IRT1*,
608 the promoter region (1,024 bp upstream of the translational start codon), the coding region, and the 3'
609 UTR sequence (310 bp downstream of the stop codon) were amplified by PCR using Phusion DNA
610 polymerase (NEB) from genomic Col-0 DNA with IRT1p_-1024F 5'-
611 CACCGACACATTAAACATTCATACCCGATT-3' and IRT1_1546R 5'-
612 CTTTAATTTACTTATCTTGAAAAAGCAGC-3'. For the mutant variants $IRT1_{S206A}$ and $IRT1_{H232A}$,
613 overlapping PCR products were generated with IRT1p_-1024F and IRT1_S198A_R 5'-
614 GATAATCCAATGACCACCGCGTGAACTATGATCCCAAG-3' or IRT1_H224A_R 5'-
615 CCATGCCTTCGAACATTTGAGCGAAGCAAAGAGCTGC-3' and IRT1_1546R and
616 IRT1_S198A_F 5'-CTTGGGATCATAGTTCACGCGGTGGTCATTGGATTATC-3' or
617 IRT1_H224A_F 5' GCAGCTCTTTGCTTCGCTCAAATGTTCGAAGGCATGG-3'. These PCR
618 products were combined in a subsequent PCR reaction using only IRT1_-1024F and IRT_1546R to
619 generate the full-length mutant variants. WT and mutant PCR products were introduced into pENTR-
620 D/TOPO (Invitrogen) and verified by Sanger sequencing before recombining into a modified
621 pMDC32 vector (Curtis and Grossniklaus, 2003) lacking the 35S promoter using LR Clonase
622 (Invitrogen) (Hanikenne et al., 2008). Plasmids were introduced into *Agrobacterium tumefaciens*
623 GV3101 by electroporation and transformed into *irt1* by floral dip (Clough and Bent, 1998).
624 Homozygous T3 seeds carrying single-locus insertions of two independent transgenic lines per
625 construct were chosen for detailed characterization based on shoot Fe concentrations in the T2
626 generation (Supplemental Table S1).
627

628 **Microarray-based transcriptomics.** All methods in this Section are described according MIAME
629 recommendations. Fifteen-d-old seedlings were used for the microarray experiment. Roots and shoots
630 were harvested separately at ZT 3 h, flash-frozen in liquid nitrogen and subsequently stored at -80°C.
631 RNA was extracted using RNeasy Plant Mini Kit with on-column DNase I digestion (Qiagen). cRNA
632 labeling and ATH1 hybridization were performed according to manufacturer's instructions at
633 GeneCore Facility, EMBL, Heidelberg. The array GeneChip ATH1-121501 (Thermo Fisher Scientific,
634 former Affymetrix), which contains 22,500 probe sets representing approximately 24,000 gene
635 sequences of the *A. thaliana* genome, was used for hybridizations. Replicate ATH1 arrays were
636 hybridized with labeled cRNA from two independent experiments, with six samples per experiment:
637 shoots or roots of WT + Fe, WT -Fe and *irt1* + Fe. Signal intensities were imported into Genespring
638 (Version 8; Agilent Technologies), and an RMA normalization was performed without transformation.
639 Differentially expressed genes (DEG) were selected by ≥ 2-fold difference in mean normalized signal
640 in both replicates and an unpaired Mann-Whitney test with Benjamini-Hochberg adjustments for
641 multiple comparisons, with a cutoff value of $P < 0.15$. The gene lists obtained with different

642 comparisons were then intersected with one another to identify overlapping DEGs using Venn
643 Selector at VIB (UGent; http:// bioinformatics.psb.ugent.be/ webtools/Venn).
644
645 **RT-qPCR.** For gene expression analysis using RT-qPCR, seedlings were grown and harvested as for
646 the microarray experiments. Total RNA was extracted from 30 to 50 mg of frozen powdered tissue
647 with Trizol Reagent following the manufacturers´ instructions. Total RNA was treated with 2 U of
648 DNase per 10 µg of total RNA using the TURBO DNA-free™ Kit (Thermo Fisher Scientific, former
649 Ambion). Integrity of DNA-free RNA was verified in Bleach Gel (Aranda et al., 2012), and
650 A280/A260 ratio in NanoDrop™ 2000/2000c (Thermo Fisher Scientific) was used to assess RNA
651 quality. One µg of DNase-treated RNA and oligo $(dT)_{18}$ primers were used in first-strand cDNA
652 synthesis with the RevertAid First Strand cDNA Synthesis Kit (Thermo Fisher Scientific) following
653 manufacturer´ instructions. RT-qPCR was performed on a LightCycler480 (Roche) in a 10-µL reaction
654 mixture containing 8 ng of cDNA, each primer at 0.25 µM and 5 µL of 2X GoTaq qPCR Master Mix
655 (Promega). The amplification program consisted of preincubation steps at 50°C for 2 min and 95°C for
656 10 min followed by 40 cycles of 95°C for 15 s and 60°C for 1 min. A final dissociation step of 95°C
657 for 10 s and 65°C for 5 s was performed for melting curve analysis. Reaction efficiencies (E) for each
658 PCR reaction were determined with the LinRegPCR program, version 2016.0 (Ruijter et al., 2009) and
659 used to calculate Transcript Level as $TL = E^{-Ct}$, with Ct as the cycle threshold. Relative TL (RTL) was
660 calculated by dividing TL of the gene of interest by geometric mean of TLs of two housekeeping
661 genes, *UBQ10* and *EF1α*. All oligonucleotide sequences are specified in Supplemental Table S3.
662
663 **Ionomics and biomass estimates.** Twenty-d-old seedlings were used for the quantification of metal
664 concentrations. Shoots and roots were harvested separately by cutting below the hypocotyl with a
665 scalpel washed in 10 mM EDTA. Root and shoot tissues were pooled per plate and desorbed by
666 washing in 5 mM $CaSO_4$, 10 mM MES-KOH, pH 5.7 for 10 min, in 5 mM $CaSO_4$, 10 mM Na_2EDTA,
667 pH 5.7 for 5 min, and twice in ultrapure water for 1 min, all carried out on ice with occasional stirring.
668 After desorbing, tissue pools were blotted dry using paper towels (Blauer Engel), and fresh biomass
669 (FW) was recorded and calculated per plant. Aliquots of 4 to 25 mg of powdered dry biomass per
670 sample were digested as described in Sinclair et al. (2017). Multi-element analysis was conducted
671 using Inductively Coupled Plasma Optical Emission Spectrometry (ICP-OES) in an iCAPDuo 6500
672 instrument (Thermo Fisher Scientific), following calibration with a blank and a series of five multi-
673 element standards from single-element standard solutions (AAS Standards; Bernd Kraft). The
674 precision of measurements was validated by measuring a sample blank and an intermediate calibration
675 standard solution, as well as digests of a certified reference material (Virginia tobacco leaves, INCT-
676 PVTL 6; Institute of Nuclear Chemistry and Technology, PL) before and after every sample series. To
677 ensure timely handling of the samples, we divided the panel of transgenic lines into two sets, each
678 representing all constructs, and we used in each experiment one set plus WT and *irt1*.

679

680 **Whole-mount staining of non-heme Fe^{III} with Perls reagent.** Seven-d-old seedlings germinated and
681 grown in standard media were harvested at ZT 1 h. Three seedlings were pooled in a 2-mL tube,
682 washed once with ice-cold 10 mM EDTA pH 5.7 for 5 min and three times with ice-cold ultrapure
683 water for 1 to 2 min. Seedlings were then submerged in 1 mL Perls solution (2% (v/v) HCl and 2%
684 (w/v) potassium ferrocyanide), vacuum infiltrated for 15 min (500 mbar) and incubated at room
685 temperature for 30 min (Roschzttardtz et al., 2009). Seedlings were then rinsed twice with ultrapure
686 water and mounted in ultrapure water for visualization on an Imager.M2 (Zeiss).

687

688 **Chlorophyll and root length measurements.** Quantification of leaf chlorophyll content and root
689 length were done on 15-d-old seedlings. For chlorophyll measurements, 34 to 52 mg of pooled shoots
690 (5 to 8 seedlings) were harvested into a 2-mL tube, flash-frozen in liquid nitrogen and homogenized
691 with a plastic pistil cooled in liquid nitrogen. After the addition of 1.5 mL 100% (v/v) methanol
692 (Sigma), samples were covered with aluminum foil and incubated at 70°C for 15 min, stirring at 850
693 rpm for 10 sec every 5 min. After cooling on ice for 5 min, methanol extracts were cleared by
694 centrifugation at 16,000x*g*, 4°C, for 1 min. Absorbance (extinction) values were measured at 652 nm
695 and 665 nm in a Synergy HTX Multi-Mode Reader (Agilent, former BioTek), using methanol as a
696 blank. Microplate pathlength correction was applied according Warren (2008). Chlorophyll
697 concentrations were calculated following Porra et al. (1989). Three repeated measurements of each
698 sample served as technical replicates. For root elongation estimates, the positions of primary root tips
699 of 10-d-old seedlings were marked with a permanent marker (Edding® 400) on the bottom of the petri
700 plate immediately after transfer to + Fe or - Fe treatment media. Five days afterwards, seedlings were
701 imaged with a Nikon Digtal SLR camera with an AF-S DX Zoom NIKKOR 18-70 mm 1:3,5-4,5G
702 ED-IF objective at 50 mm distance. Primary root length was measured using ImageJ (Schneider et al.,
703 2012) by drawing a segmented line along the main root.

704

705 **Root surface Ferric Chelate Reductase (FCR) activity assays.** Seedlings were grown as for
706 microarray experiments. Roots of 5 to 8 15-d-old seedlings (8 to 33 mg fresh biomass) were harvested
707 at ZT 3 h using a scalpel, pooled and immediately transferred to 2-mL tubes securely capped to avoid
708 humidity loss. Roots were incubated in 1.5 mL of assay solution (0.1 mM Fe^{III}EDTA, 0.3 mM
709 FerroZine) at RT in darkness for 20 min (time course experiment) or 40 min (FCR activity after Fe
710 deficiency for 5 d). After reading absorbance at 535 nm on a PowerWave XS2 plate reader (Agilent,
711 former BioTek), Fe^{II}FerroZine concentrations were calculated using an extinction coefficient of 28.6
712 mM^{-1} cm^{-1} (Gibbs, 1976).

713

714 **IRT1 Immunoblots.** Total protein was extracted from 30 mg FW of pooled root tissues as described
715 earlier (Sgula et al., 2008) with the difference that 2% (w/v) DTT was used as reducing agent and that

716 prior to centrifugation, protein extracts were incubated 5 min at room temperature (RT) to facilitate
717 membrane solubilization. Total protein in the supernatants was quantified in 1:5 dilutions with the
718 Pierce™ BCA Protein Assay Kit using BSA as a standard. Per sample, 20 µg of total protein was
719 mixed with ultrapure water and 2 µL of 6x loading buffer (375 mM Tris-HCl (pH 6.8), 30% (v/v)
720 mercaptoethanol, 0.03% (v/v) bromophenol blue, 12% (w/v) SDS, and 60% (v/v) glycerol) in a final
721 volume of 12 µL and subsequently incubated for 20 min at 37°C. Proteins were separated by 12%
722 (w/v) SDS-PAGE and blotted onto a polyvinylidene difluoride (PVDF) membrane by wet/tank
723 transfer (Towbin et al., 1979). The PVDF membrane was blocked with 5% (w/v) skim milk in TBS-T
724 (0.05% Tween-20) at RT for 1 h and probed with anti-IRT1 antibody (1:5,000, Agrisera AS111780,
725 Lot number 1203) in 2.5% (w/v) skim milk in TBS-T (0.05% Tween-20) at RT for 1 h. Following
726 incubation at RT for 1 h with the secondary antibody goat anti-rabbit IgG (H+L), HRP (1:20,000,
727 Thermo Fisher Scientific 31466; lot number RL243150) in 2.5% (w/v) skim milk in TBS-T, signals
728 were detected with ECL Select Western Blotting Detection Reagent (GE Healthcare) and a Fusion Fx7
729 documentation system (Vilber Lourmat).
730
731 **Short-term uptake rates of ^{55}Fe.** Hydroponically cultivated 7.5- (WT and *irt1* IRT1) or 8.5- (*irt1*,
732 *irt1* S206A and *irt1* H232A) week-old plants of equal sizes were used for short-term Fe uptake assays.
733 To allow for accurate sample processing we included one line per construct, WT and *irt1* in each
734 experiment. At ZT 1 h, the root systems of 4 to 5 replicate plants per line were submerged in glass
735 liquid scintillation vials (one plant per vial) containing 35 mL of 1 mM MES-KOH pH 5.7, 2.1 µM
736 citrate, 1 mM ascorbic acid and 2 µM ^{55}Fe ($^{55}FeCl_3$, 0.0197 MBq nmol^{-1}, Perkin-Elmer). After two
737 incubations of 1.5 min and 15 min duration for each genotype, respectively, roots were desorbed by
738 washing 3 times in fresh ice-cold solution of 5 mM $CaSO_4$, 10 mM Na_2EDTA (pH 5.7), 1 mM MES-
739 KOH (pH 5.7) for 5 min (40 mL per plant). Roots were cut off, carefully blotted dry between paper
740 towels (Blauer Engel), weighed and stored at -20°C for 24 hours in 6 ml HPDE scintillation vials to
741 destroy the cells. Roots were then suspended in 4 mL of a scintillation cocktail at RT (Rotiszint, Carl
742 Roth, Germany). Counting was performed twice for each sample (10 min per sample) with a ß-
743 scintillation counter Beckman LS6000TA (Beckman Coulter, USA). Roots of two plants identically
744 grown and processed but not exposed to the incubation solution were used to determine background
745 counts. For calculation of ^{55}Fe uptake, values of uptake after 1.5 min were subtracted from those after
746 15 min uptake and expressed as nmol ^{55}Fe g^{-1} FW h^{-1}. Pre-cultivation periods and conditions were
747 slightly varied from experiment to experiment, gradually obtaining plants of more and more equivalent
748 sizes and developmental stages for all genotypes. For a confirmation experiment at MU (Supplemental
749 Table S2), plants of similar size grown hydroponically were pre-incubated in 35 mL of a solution of
750 0.2 mM $CaSO_4$, 1 mM ascorbic acid, 5 mM MES-TRIS, pH 5.0, for 30 min, and then transferred to 30
751 mL of uptake buffer of identical composition with the addition of 1 µM $FeCl_3$ (spiked with *ca.* 2 µCi
752 ^{59}Fe) for an uptake period of 120 min. Washing solutions were composed as follows: 20 mM TRIS, 5

753 mM EDTA (30 mL for 10 min, followed by 35 mL for 10 min), ultrapure water (25 mL for 5 min,
754 twice). Roots were separated from shoots and blotted dry as described above before scintillation
755 counting. Vials containing only scintillation cocktail were used for background subtraction.
756
757 **Statistical analysis.** Statistical analyses were conducted in R Studio Version 1.1.456 (R Core Team,
758 2020). Two-factor ANOVA was performed assuming the following linear model: model = lm (Var1 ~
759 TREATMENT + GENOTYPE + TREATMENT:GENOTYPE). Tukey HSD was applied in multiple
760 comparisons of means. Alternatively, when homoscedasticity was not met ($P < 0.05$, Levene's test),
761 pairwise Welch *t*-tests were conducted. When normality was not met ($P < 0.05$, Shapiro-Wilk test),
762 pairwise Student's *t*-tests were used. For all *t*-tests, pairwise differences were considered significant
763 when FDR-corrected $q < 0.05$.
764
765 **Accession numbers**
766 Sequence data for the genes mentioned in the text can be found on The Arabidopsis Genome Initiative
767 (TAIR) or GenBank website. Accession numbers are (in alphabetic order): *ALTERNATIVE*
768 *OXIDASE1A* (*AOX1A*), *AT3G22370*; *basic HELIX LOOP HELIX39* (*bHLH39*), *AT3G56980*; *basic*
769 *HELIX LOOP HELIX 101* (*bHLH101*), *AT5G04150*; *BETA-GLUCOSIDASE42* (*BGLU42*),
770 *AT5G36890*; *BETA-GLUCOSIDASE45* (*BGLU45*), *BRUTUS-LIKE2* (*BTSL2*), *AT1G18910*;
771 *AT1G61810*; *CYTOCHROME P45071b5* (*CYP71B5*), *AT3G53280*; *DETOXIFICATION1* (*DTX1*),
772 *AT2G04040*; *FERRITIN1* (*FER1*), *AT5G01600*; *IRONMAN1* (*IMA1*), *AT1G47400*; *IRON*
773 *REGULATED TRANSPORTER1* (*IRT1*), *AT4G19690*; *IRON REGULATED TRANSPORTER2* (*IRT2*),
774 *AT4G19680*; *MYB DOMAIN PROTEIN10* (*MYB10*), *AT3G12820*; *MYB DOMAIN PROTEIN 72*
775 (*MYB72*), *AT1G56160*; *NICOTIANAMINE SYNTHASE4* (*NAS4*), *AT1G56430*; *ZRT/IRT-LIKE*
776 *PROTEIN 2* (*ZIP2*), *AT5G59520*; *ZINC-INDUCED FACILITATOR1* (*ZIF1*), *AT5G13740*. The
777 microarray data set accession number is xxx (https://www.ncbi.nlm.nih. gov/geo/).
778
779 **SUPPLEMENTAL MATERIAL**
780 **Supplemental Figure S1.** Details of the *irt1* phenotype.
781 **Supplemental Figure S2.** Topology model of IRT1 highlighting the amino acid residues mutated in
782 this paper.
783 **Supplemental Figure S3.** Details of *IRT1* expression in transport-inactive mutants.
784 **Supplemental Figure S4.** Photographs of Arabidopsis WT, *irt1*, *irt1* IRT1, *irt1* S206A, *irt1* H232A
785 plants.
786 **Supplemental Figure S5.** Root Fe concentration, total Fe per plant, root Mn concentration and
787 *NRAMP1* expression.
788 **Supplemental Figure S6.** Fe deficiency responses are not constitutively activated in shoots of *irt1*
789 S206A lines.

790 **Supplemental Figure S7.** Experimental rationale of transcriptomic analysis.
791 **Supplemental Figure S8.** Validation of microarray data using RT-qPCR.
792 **Supplemental Figure S9.** Lack of Fe-deficiency response in cortex-enriched transcripts in the *irt1*
793 mutant.
794 **Supplemental Figure S10.** Transcript levels of candidate genes for roles in IRT1-dependent root-to-
795 shoot translocation across genotypes.
796 **Supplemental Table S1.** Fe concentrations in shoots of independent transgenic lines for *irt1* IRT1,
797 *irt1* S206A and *irt1* H232A.
798 **Supplemental Table S2.** Short-term uptake of radiolabeled Fe into roots of Fe-deficient wild-type and
799 *irt1* mutant plants.
800 **Supplemental Table S3.** Oligonucleotides used in the present study.
801
802 **LARGE DATASETS**
803 **Supplemental Dataset S1.** List of overlapping differentially expressed genes between -Fe *vs*. C (WT)
804 and *irt1* (C) *vs*. WT (-Fe) in roots (**, *; Fig. 7A, B).
805 **Supplemental Dataset S2.** List of differentially expressed genes that overlap between -Fe *vs*. C (WT)
806 and *irt1 vs*. WT (C) in roots (#; Fig. 7A, B).
807 **Supplemental Dataset S3.** List of overlapping differentially expressed genes between -Fe *vs*. C (WT)
808 and *irt1* (C) *vs*. WT (-Fe) in shoots (**, *; Fig. 7C, D).
809 **Supplemental Dataset S4.** List of differentially expressed genes that overlap between -Fe *vs*. C (WT)
810 and *irt1 vs*. WT (C) in shoots (#; Fig. 7C, D).
811 **Supplemental Dataset S5.** List of transcripts reported at higher or lower abundance in the stele *vs*. the
812 cortex that were Fe deficiency-responsive according to this study.
813 **Supplemental Dataset S6.** List of transcripts reported at higher or lower abundance in the stele *vs*. the
814 endodermis that were Fe deficiency-responsive according to this study.
815
816 **Acknowledgments**
817 The *fet3fet4* and corresponding wild-type yeast strains were kindly provided by Prof. Dr.
818 David Eide (University of Wisconsin-Madison, US), Arabidopsis *pam42* by Prof. Dr. Dario
819 Leister (LM University Munich, Germany). We are grateful to Petra Düchting for multi-
820 element analysis, Dr. Lara Syllwasschy for *t*-test scripts, Andreas Aufermann and Iris Sandorf
821 for technical assistance in plant cultivation, and all lab members for comments (Ruhr
822 University Bochum, Germany). We also thank María de los Ángeles and Patricia Lorente for
823 technical support, and Rafael Picorel for providing infrastructure (EEAD, CSIC, Spain).
824
825 **FIGURE LEGENDS**

826 **Figure 1. The *irt1* mutant overaccumulates Fe in the root whereas the shoot is Fe-limited. (A)**
827 Photographs of 20-d-old WT and *irt1* seedlings grown in Fe-sufficient (+ Fe, 10 µM FeHBED) and
828 Fe-deficient (- Fe, 0 µM FeHBED) agar-solidified 0.25x modified Hoagland's medium (EDTA-
829 washed agar) for 10 d, subsequent to an initial cultivation in standard medium (5 µM FeHBED,
830 unwashed agar) for 10 d, on vertically oriented petri plates. **(B - D)** Shoot **(B)** and root **(C)** Fe
831 concentrations and root:shoot Fe concentration ratio **(D)** in 20-d-old WT and *irt1* seedlings. Seedlings
832 were grown as in **(A)**. Bars represent arithmetic mean ± SD (n = 3 pools of tissue, each from 15 (WT)
833 or 30 (*irt1*) seedlings, with 15 seedlings cultivated per plate). Distinct letters indicate statistically
834 significant differences (P < 0.05, two-way ANOVA followed by Tukey´s HSD test). Data show one
835 experiment representative of three independent experiments. DW: dry biomass.
836
837 **Figure 2. Fe accumulates in sub-epidermal cell layers of *irt1* roots. (A)** Histochemical detection of
838 labile $Fe^{(+II, +III)}$ by Perls stain in the root differentiation zone of 7-d-old WT, *irt1* and *frd3-7* seedlings
839 grown on agar-solidified 0.25x modified Hoagland's medium (5 µM FeHBED). **(B)** Magnified image
840 (20x) of WT and *irt1* roots shown in **(A)**. Photographs are representative of n = 10 to 12 roots from
841 two independent experiments, each with seedlings cultivated on three replicate petri plates processed
842 in parallel. Scale bars: 100 µm **(A)**, 50 µm **(B)**.
843
844 **Figure 3. Fe transport-inactive $IRT1_{S206A}$ partially complements *irt1*. (A - D)** Immunoblot
845 detection of IRT1 protein **(A)**, photographs **(B)**, leaf chlorophyll concentrations **(C)** and mean root
846 elongation over the last 5 d of growth **(D)** in 15-d-old seedlings of WT, *irt1*, *irt1* IRT1, *irt1* S206A and
847 *irt1* H232A. Seedlings were grown on Fe-sufficient (+ Fe, 10 µM FeHBED) and Fe-deficient (- Fe, 0
848 µM FeHBED) agar-solidified 0.25x modified Hoagland's medium (EDTA-washed agar) for 5 d,
849 subsequent to an initial cultivation period of 10 d in standard medium (5 µM Fe-HBED; unwashed
850 agar), on vertically oriented petri plates. Total root protein extracts (20 µg) were separated on
851 denaturing gels and blotted onto PVDF membranes, with the Commassie Blue-stained (CB) PVDF
852 membrane shown as loading control **(A)**. Bars represent arithmetic mean ± SD (n = 4 pools of 5 to 8
853 shoots **(C)**; n = 8 to 10 roots **(D)**). Distinct letters indicate significant differences (P < 0.05) according
854 to two-sample Student's or Welch t-tests upon correction for multiple comparisons **(C)** or two-way
855 ANOVA followed by Tukey´s HSD test **(D)**. Images in **(A)** are representative of three replicate
856 membranes. Data are from two independent experiments, each with two **(C)** or one **(D)** replicate
857 plates.
858
859 **Figure 4. Yeast complementation assay and root $^{55}Fe^{2+}$ uptake rates. (A)** Growth of WT and the
860 *fet3fet4* Fe transport-defective mutant transformed with a modified pFL61 plasmid as empty vector
861 (eV), or containing the *IRT1*, $IRT1_{S206A}$ or $IRT1_{H232A}$ cDNA, respectively. Ten-fold serial dilutions of
862 liquid cultures were spotted on SD (-Ura) medium (pH 5.7) supplemented with 0.5 mM $FeSO_4$ or left

863 unamended. **(B)** Uptake rates determined in hydroponically cultivated 7.5 to 8.5-w-old plants over a
864 13.5-min period. Before the initiation of uptake assays, plants were exposed to Fe deficiency (0 µM
865 FeHBED) for 6 d, subsequent to an initial cultivation period in 1x modified Hoagland‘s solution
866 containing 10 µM FeHBED (WT and *irt1* IRT1) or 50 µM FeHBED (all other genotypes) for 6 to 7
867 weeks. Bars represent arithmetic mean ± SD (n = 4 to 5 plants). Data show one
868 experiment representative of three independent experiments (see Supplemental Table S2).
869
870 **Figure 5. Partial rescue of root-to-shoot Fe allocation in *irt1* S206A. (A - F)** Shoot Fe
871 concentration **(A and B)**, shoot Fe allocation **(C and D)** and shoot Mn concentrations **(E and F)** in 20-
872 d-old seedlings of WT, *irt1*, *irt1* IRT1, *irt1* S206A and *irt1* H232A grown on Fe-sufficient (+ Fe, 10
873 µM FeHBED) and Fe-deficient (- Fe, 0 µM FeHBED) agar-solidified 0.25x modified Hoagland's
874 medium (EDTA-washed agar) for 10 d, subsequent to an initial cultivation period of 10 d in standard
875 medium (5 µM FeHBED; unwashed agar), on vertically oriented petri plates. Bars represent arithmetic
876 mean ± SD (n = 3 pools of tissues, each from 15 to 30 seedlings, with 15 seedlings cultivated per
877 plate). Distinct letters indicate significant differences ($P < 0.05$) according to two-sample Student's t-
878 tests upon correction for multiple comparisons **(A - D)** or in two-way ANOVA followed by Tukey´s
879 HSD test **(E and F)**. Data show one experiment representative of two independent experiments.
880
881 **Figure 6. *FER1* transcript levels. (A - C)** Relative transcript levels (RTL) of *FER1* in shoots **(A)** and
882 roots **(B)** of 15-d-old WT, *irt1*, *irt1* IRT1, *irt1* S206A, *irt1* H232A seedlings. RTL are shown
883 normalized to both *UBQ10* and *EF1α* as constitutively expressed control genes. Seedlings were grown
884 on Fe-sufficient (+ Fe, 10 µM FeHBED) and Fe-deficient (- Fe, 0 µM FeHBED) agar-solidified 0.25x
885 modified Hoagland's medium (EDTA-washed agar) for 5 d, subsequent to an initial cultivation period
886 of 10 d in standard medium (5 µM FeHBED; unwashed agar), on vertically oriented petri plates. Bars
887 represent arithmetic mean ± SD (n = 6 technical replicates on cDNA obtained using tissue pooled from
888 2 to 3 plates, each with 20 seedlings). Distinct letters indicate significant differences ($P < 0.05$)
889 according to two-sample Student's or Welch t-tests upon correction for multiple comparisons. Data
890 show one experiment representative of three independent experiments.
891
892 **Figure 7. Transcriptome analysis of *irt1* compared to Fe-deficient and -sufficient WT seedlings.**
893 **(A - D)** Summary of microarray-based transcriptome data in roots **(A and B)** and shoots **(C and D)**.
894 Shown within Venn diagrams are the numbers of genes with ≥ 2-fold differences in transcript levels in
895 different comparisons ($P < 0.15$). Colors denote responses, (red/blue, higher/lower transcript
896 abundance in one genotype and/or condition compared to the other). Symbols denote Fe deficiency-
897 responsive transcripts that are deregulated (*, **) or not (#) in *irt1*. **(E)** Relative transcript levels
898 (RTL) of *MYB10* and *MYB72* in roots of WT and *irt1* seedlings. RTL are shown normalized to
899 *UBQ10*. **(F)** Heat map of *MYB72* and *MYB10* transcript abundance - Fe *vs*. + Fe in roots of different

genotypes as indicated. Numbers are Log_2 (transcript level ratios, with RTL normalized to both *UBQ10* and *EF1α*), and raw *z*-score for each gene was used to scale the heat map, from three independent experiments. WT and *irt1* seedlings were grown on Fe-sufficient (+ Fe, 10 µM FeHBED) and Fe-deficient (- Fe, 0 µM FeHBED) agar-solidified modified 0.25x Hoagland's medium (EDTA-washed agar) for 5 d, subsequent to an initial cultivation period of 10 d in standard medium (5 µM FeHBED; unwashed agar), on vertically oriented petri plates **(A - F)**. Bars represent arithmetic mean ± SD (n = 3 technical replicates on cDNA obtained using tissue pooled from 2 to 3 plates, each with 20 seedlings **(E)**). Distinct letters indicate significant differences ($P < 0.05$) in two-way ANOVA followed by Tukey´s HSD test (*MYB10*) or two-sample Student's *t*-tests upon correction for multiple comparisons (*MYB72*). Data in **(F)** are from three independent experiments.

Parsed Citations

Alberts B, Johnson A, Lewis J, et al (2002) The evolution of electron-transport chains in molecular biology of the cell. 4th edition. New York: Garland Science. Available from: https://www.ncbi.nlm.nih.gov/books/NBK26849/
Google Scholar: Author Only Title Only Author and Title

Aranda PS, LaJoie DM, Jorcyk CL (2012) Bleach gel: A simple agarose gel for analyzing RNA quality. Electrophoresis 33: 366–369
Google Scholar: Author Only Title Only Author and Title

Barberon M, Vermeer JEM, Bellis DD, Wang P, Naseer S, Andersen TG, Humbel BM, Nawrath C, Takano J, Salt DE, et al (2016) Adaptation of root function by nutrient-induced plasticity of endodermal differentiation. Cell 164: 447–59
Google Scholar: Author Only Title Only Author and Title

Barberon M, Dubeaux G, Kolb C, Isono E, Zelazny E, Vert G (2014) Polarization of IRON-REGULATED TRANSPORTER1 (IRT1) to the plant-soil interface plays crucial role in metal homeostasis. Proc Natl Acad Sci USA 111: 8293–8
Google Scholar: Author Only Title Only Author and Title

Barberon M, Zelazny E, Robert S, Conéjéro G, Curie C, Friml J, Vert G (2011) Monoubiquitin-dependent endocytosis of the IRON-REGULATED TRANSPORTER1 (IRT1) transporter controls iron uptake in plants. Proc Natl Acad Sci USA 108: E450–E458
Google Scholar: Author Only Title Only Author and Title

Bauer P, Ling H-Q, Guerinot M (2007) FIT, the FER-like iron deficiency induced transcription factor in Arabidopsis. Plant Physiol Biochem 45: 260–261
Google Scholar: Author Only Title Only Author and Title

Baxter IR, Vitek O, Lahner B, Muthukumar B, Borghi M, Morrissey J, Guerinot ML, Salt DE (2008) The leaf ionome as a multivariable system to detect a plant's physiological status. Proc Natl Acad Sci USA 105: 12081–12086
Google Scholar: Author Only Title Only Author and Title

Brady SM, Orlando DA, Lee J-Y, Wang JY, Koch J, Dinneny JR, Mace D, Ohler U, Benfey PN (2007) A high-resolution root spatiotemporal map reveals dominant expression patterns. Science 318: 801–806
Google Scholar: Author Only Title Only Author and Title

Becher M, Talke IN, Krall L, Krämer U (2004) Cross-species microarray transcript profiling reveals high constitutive expression of metal homeostasis genes in shoots of the zinc hyperaccumulator Arabidopsis halleri. Plant J 37: 251–68
Google Scholar: Author Only Title Only Author and Title

Briat J-F, Duc C, Ravet K, Gaymard F (2009) Ferritins and iron storage in plants. Biochim Biophys Acta 1800: 806–14
Google Scholar: Author Only Title Only Author and Title

Buckhout TJ, Yang TJW, Schmidt W (2009) Early iron-deficiency-induced transcriptional changes in Arabidopsis roots as revealed by microarray analyses. BMC Genomics 10: 147
Google Scholar: Author Only Title Only Author and Title

Cailliatte R, Schikora A, Briat J-F, Mari S, Curie C (2010) High-affinity manganese uptake by the metal transporter NRAMP1 is essential for Arabidopsis growth in low manganese conditions. Plant Cell 22: 904–17
Google Scholar: Author Only Title Only Author and Title

Castaings L, Caquot A, Loubet S, Curie C (2016) The high-affinity metal transporters NRAMP1 and IRT1 team up to take up iron under sufficient metal provision. Sci Rep 6: 37222
Google Scholar: Author Only Title Only Author and Title

Chaney RL (1988) Plants can utilize iron form Fe-N,N'-di-(2-hydroxybenzoyl)-ethylenediamine-N,N'-diacetic acid, a ferric chelate with 106 greater formation constant than Fe-EDDHA. J Plant Nutr 11: 1033–1050
Google Scholar: Author Only Title Only Author and Title

Chapelle A, Morreel K, Vanholme R, Le-Bris P, Morin H, Lapierre C, Boerjan W, Jouanin L, Demont-Caulet N (2012) Impact of the absence of stem-specific β-Glucosidases on lignin and monolignols. Plant Physiol 160: 1204–1217
Google Scholar: Author Only Title Only Author and Title

Clough SJ, Bent AF (1998) Floral dip: a simplified method for Agrobacterium-mediated transformation of Arabidopsis thaliana. Plant J 16: 735–43
Google Scholar: Author Only Title Only Author and Title

Colangelo EP, Guerinot ML (2004) The Essential Basic Helix-Loop-Helix Protein FIT1 is required for the iron deficiency response. Plant Cell 16: 3400–3412
Google Scholar: Author Only Title Only Author and Title

Connolly EL, Campbell NH, Grotz N, Prichard CL, Guerinot M (2003) Overexpression of the FRO2 Ferric Chelate Reductase confers tolerance to growth on low iron and uncovers posttranscriptional control. Plant Physiol 133: 1102–1110
Google Scholar: Author Only Title Only Author and Title

Connolly EL, Fett JP, Guerinot ML (2002) Expression of the IRT1 metal transporter is controlled by metals at the levels of transcript

and protein accumulation. Plant Cell 14: 1347–57
Google Scholar: Author Only Title Only Author and Title

Curtis MD, Grossniklaus U (2003) A Gateway Cloning Vector Set for High-Throughput Functional Analysis of Genes in Planta. Plant Physiol 133: 462–469
Google Scholar: Author Only Title Only Author and Title

Desbrosses-Fonrouge A-G, Voigt K, Schröder A, Arrivault S, Thomine S, Krämer U (2005) Arabidopsis thaliana MTP1 is a Zn transporter in the vacuolar membrane which mediates Zn detoxification and drives leaf Zn accumulation. FEBS Lett 579: 4165–4174
Google Scholar: Author Only Title Only Author and Title

Dinneny JR, Long TA, Wang JY, Jung JW, Mace D, Pointer S, Barron C, Brady SM, Schiefelbein J, Benfey PN (2008) Cell identity mediates the response of Arabidopsis roots to abiotic stress. Science 320: 942–5
Google Scholar: Author Only Title Only Author and Title

Dix DR, Bridgham JT, Broderius MA, Byersdorfer CA, Eide DJ (1994) The FET4 gene encodes the low affinity Fe(II) transport protein of Saccharomyces cerevisiae. J Biol Chem 269: 26092–9
Google Scholar: Author Only Title Only Author and Title

Dohmen RJ, Strasser AWM, Höner CB, Hollenberg CP (1991) An efficient transformation procedure enabling long-term storage of competent cells of various yeast genera. Yeast 7: 691–692
Google Scholar: Author Only Title Only Author and Title

Dubeaux G, Neveu J, Zelazny E, Vert G (2018) Metal Sensing by the IRT1 transporter-receptor orchestrates its own degradation and plant metal nutrition. Mol Cell 69: 953-964.e5
Google Scholar: Author Only Title Only Author and Title

Eide D, Broderius M, Fett J, Guerinot ML (1996) A novel iron-regulated metal transporter from plants identified by functional expression in yeast. Proc Natl Acad Sci USA 93: 5624–8
Google Scholar: Author Only Title Only Author and Title

Gao F, Robe K, Bettembourg M, Navarro N, Rofidal V, Santoni V, Gaymard F, Vignols F, Roschzttardtz H, Izquierdo E, Dubos C (2020a) The Transcription Factor bHLH121 interacts with bHLH105 (ILR3) and its closest homologs to regulate iron homeostasis in Arabidopsis. Plant Cell 32: 508
Google Scholar: Author Only Title Only Author and Title

Gao F, Robe K, Dubos C (2020b) Further insights into the role of bHLH121 in the regulation of iron homeostasis in Arabidopsis thaliana. Plant Signal Behav 15: 1795582
Google Scholar: Author Only Title Only Author and Title

Gibbs CR (1976) Characterization and application of FerroZine iron reagent as a ferrous iron indicator. Anal Chem 48: 1197–1201
Google Scholar: Author Only Title Only Author and Title

Giehl R, Lima JE, von Wirén N (2012) Localized iron supply triggers lateral root elongation in Arabidopsis by altering the AUX1-mediated auxin distribution. Plant Cell 24: 33–49
Google Scholar: Author Only Title Only Author and Title

Green LS, Rogers EE (2004) FRD3 Controls iron localization in Arabidopsis. Plant Physiol 136: 2523–2531
Google Scholar: Author Only Title Only Author and Title

Hanikenne M, Talke IN, Haydon M, Lanz C, Nolte A, Motte P, Kroymann J, Weigel D, Krämer U (2008) Evolution of metal hyperaccumulation required cis-regulatory changes and copy number expansion of HMA4. Nature 453: 391-4
Google Scholar: Author Only Title Only Author and Title

Haydon MJ, Cobbett CS (2007) A Novel Major Facilitator Superfamily Protein at the Tonoplast Influences Zinc Tolerance and Accumulation in Arabidopsis. Plant Physiol 143: 1705–1719
Google Scholar: Author Only Title Only Author and Title

Haydon MJ, Kawachi M, Wirtz M, Hillmer S, Hell R, Krämer U (2012) Vacuolar nicotianamine has critical and distinct roles under iron deficiency and for zinc sequestration in Arabidopsis. Plant Cell 24: 724–37
Google Scholar: Author Only Title Only Author and Title

Henriques R, Jásik J, Klein M, Martinoia E, Feller U, Schell J, Pais MS, Koncz C (2002) Knock-out of Arabidopsis metal transporter gene IRT1 results in iron deficiency accompanied by cell differentiation defects. Plant Mol Biol 50: 587-597
Google Scholar: Author Only Title Only Author and Title

Ivanov R, Brumbarova T, Blum A, Jantke AM, Fink-Straube C, Bauer P (2014) SORTING NEXIN1 is required for modulating the trafficking and stability of the Arabidopsis IRON-REGULATED TRANSPORTER1. Plant Cell 26: 1294-1307
Google Scholar: Author Only Title Only Author and Title

Jakoby M, Wang H-Y, Reidt W, Weisshaar B, Bauer P (2004) FRU (BHLH029) is required for induction of iron mobilization genes in Arabidopsis thaliana. FEBS letters 577: 528–534
Google Scholar: Author Only Title Only Author and Title

Kerkeb L, Mukherjee I, Chatterjee I, Lahner B, Salt DE, Connolly EL (2008) Iron-induced turnover of the Arabidopsis IRON-REGULATED TRANSPORTER1 metal transporter requires lysine residues. Plant Physiol 146: 1964–73
Google Scholar: Author Only Title Only Author and Title

Khan MA, Castro-Guerrero NA, McInturf SA, Nguyen NT, Dame AN, Wang J, Bindbeutel RK, Joshi T, Jurisson SS, Nusinow DA, et al (2018) Changes in iron availability in Arabidopsis are rapidly sensed in the leaf vasculature and impaired sensing leads to opposite transcriptional programs in leaves and roots. Plant Cell Environ 41: 2263–2276
Google Scholar: Author Only Title Only Author and Title

Kim SA, LaCroix IS, Gerber SA, Guerinot M (2019) The iron deficiency response in Arabidopsis thaliana requires the phosphorylated transcription factor URI. Proc Natl Acad Sci USA 201916892
Google Scholar: Author Only Title Only Author and Title

Kobayashi T, Nishizawa NK (2012) Iron uptake, translocation, and regulation in higher plants. Annu Rev Plant Biol 63: 131–152
Google Scholar: Author Only Title Only Author and Title

Lei R, Li Y, Cai Y, Li C, Pu M, Lu C, Yang Y, Liang G (2020) bHLH121 Functions as a direct link that facilitates the activation of FIT by bHLH IVc Transcription Factors for maintaining Fe homeostasis in Arabidopsis. Mol Plant 13: 634-649
Google Scholar: Author Only Title Only Author and Title

Lopez A, Cacoub P, Macdougall IC, Peyrin-Biroulet L (2016) Iron deficiency anaemia. Lancet 387: 907–916
Google Scholar: Author Only Title Only Author and Title

Marquès-Bueno MD, Morao AK, Cayrel A, Platre MP, Barberon M, Caillieux E, Colot V, Jaillais Y, Roudier F, Vert G (2016) A versatile Multisite Gateway-compatible promoter and transgenic line collection for cell type-specific functional genomics in Arabidopsis. Plant J 85: 320–333
Google Scholar: Author Only Title Only Author and Title

Martín-Barranco A, Spielmann J, Dubeaux G, Vert G, Zelazny E (2020) Dynamic control of the high-affinity iron uptake complex in root epidermal cells. Plant Physiol 184: 1236
Google Scholar: Author Only Title Only Author and Title

Mendoza-Cózatl DG, Xie Q, Akmakjian GZ, Jobe TO, Patel A, Stacey MG, Song L, Demoin DW, Jurisson SS, Stacey G, Schroeder JI (2014) OPT3 is a component of the iron-signaling network between leaves and roots and misregulation of OPT3 leads to an over-accumulation of cadmium in seeds. Mol Plant 7: 1455-1469
Google Scholar: Author Only Title Only Author and Title

Palmer CM, Hindt MN, Schmidt H, Clemens S, Guerinot M (2013) MYB10 and MYB72 are required for growth under iron-limiting conditions. PLoS Genet 9: e1003953
Google Scholar: Author Only Title Only Author and Title

Porra RJ, Thompson WA, Kriedemann PE (1989) Determination of accurate extinction coefficients and simultaneous equations for assaying chlorophylls a and b extracted with four different solvents: verification of the concentration of chlorophyll standards by atomic absorption spectroscopy. Biochimica et Biophysica Acta (BBA) - Bioenergetics 975: 384-394
Google Scholar: Author Only Title Only Author and Title

R Core Team (2020) R: A language and environment for statistical computing. R Foundation for Statistical Computing, Vienna, Austria. URL http://www.R-project.org/
Google Scholar: Author Only Title Only Author and Title

Rodríguez-Celma J, Connorton JM, Kruse I, Green RT, Franceschetti M, Chen Y-T, Cui Y, Ling H-Q, Yeh K-C, Balk J (2019) Arabidopsis BRUTUS-LIKE E3 ligases negatively regulate iron uptake by targeting transcription factor FIT for recycling. Proc Natl Acad Sci USA 116: 17584–17591
Google Scholar: Author Only Title Only Author and Title

Rogers EE, Eide DJ, Guerinot M (2000) Altered selectivity in an Arabidopsis metal transporter. Proc Natl Acad Sci USA 97: 12356–12360
Google Scholar: Author Only Title Only Author and Title

Roschzttardtz H, Conéjéro G, Curie C, Mari S (2009) Identification of the Endodermal Vacuole as the Iron Storage Compartment in the Arabidopsis Embryo. Plant Physiol 151: 1329–1338
Google Scholar: Author Only Title Only Author and Title

Ruijter JM, Ramakers C, Hoogaars WMH, Karlen Y, Bakker O, Hoff MJB van den, Moorman AFM (2009) Amplification efficiency: linking baseline and bias in the analysis of quantitative PCR data. Nucleic Acids Res 37: e45–e45
Google Scholar: Author Only Title Only Author and Title

Salomé PA, Bernal M, Krämer U (2014) Plant Circadian Networks, Methods and Protocols. Methods Mol Biology 1158: 227–238
Google Scholar: Author Only Title Only Author and Title

Schmid NB, Giehl RFH, Döll S, Mock H-P, Strehmel N, Scheel D, Kong X, Hider RC, von Wirén N (2014) FERULOYL-COA 6′-HYDROXYLASE1-dependent coumarins mediate iron acquisition from alkaline substrates in Arabidopsis. Plant Physiol 164: 160-172
Google Scholar: Author Only Title Only Author and Title

Schneider CA, Rasband WS, Eliceiri KW (2012) NIH Image to ImageJ: 25 years of image analysis. Nat Methods 9: 671–675

Google Scholar: Author Only Title Only Author and Title

Schulten A, Krämer U (2017) Interactions Between Copper Homeostasis and Metabolism in Plants. In: Cánovas F., Lüttge U., Matyssek R. (eds) Progress in Botany Vol. 79. Progress in Botany, vol 79. Springer, Cham. https://doi.org/10.1007/124_2017_7
Google Scholar: Author Only Title Only Author and Title

Schwarz B, Bauer P (2020) FIT, a regulatory hub for iron deficiency and stress signaling in roots, and FIT-dependent and -independent gene signatures. J Exp Bot 71: 1694-1705
Google Scholar: Author Only Title Only Author and Title

Sgula M, Briat J-F, Vert G, Curie C (2008) Cytokinins negatively regulate the root iron uptake machinery in Arabidopsis through a growth-dependent pathway. Plant J 55: 289–300
Google Scholar: Author Only Title Only Author and Title

Shin L-J, Lo J-C, Chen G-H, Callis J, Fu H, Yeh K-C (2013) IRT1 degradation factor1, a ring E3 ubiquitin ligase, regulates the degradation of IRON-REGULATED TRANSPORTER1 in Arabidopsis. Plant Cell 25: 3039–51
Google Scholar: Author Only Title Only Author and Title

Sinclair SA, Larue C, Bonk L, Khan A, Castillo-Michel H, Stein RJ, Grolimund D, Begerow D, Neumann U, Haydon MJ, et al (2017) Etiolated Seedling Development Requires Repression of Photomorphogenesis by a Small Cell-Wall-Derived Dark Signal. Curr Biol 27: 3403-3418.e7
Google Scholar: Author Only Title Only Author and Title

Sivitz A, Grinvalds C, Barberon M, Curie C, Vert G (2011) Proteasome-mediated turnover of the transcriptional activator FIT is required for plant iron-deficiency responses. Plant J 66: 1044–1052
Google Scholar: Author Only Title Only Author and Title

Sivitz AB, Hermand V, Curie C, Vert G (2012) Arabidopsis bHLH100 and bHLH101 control iron homeostasis via a FIT-independent pathway. PLoS One 7: e44843
Google Scholar: Author Only Title Only Author and Title

Stringlis IA, Yu K, Feussner K, Jonge R de, Bentum S, Verk MC, Berendsen RL, Bakker PA, Feussner I, Pieterse CM (2018) MYB72-dependent coumarin exudation shapes root microbiome assembly to promote plant health. Proc Natl Acad Sci USA 115: 201722335
Google Scholar: Author Only Title Only Author and Title

Thieme CJ, Rojas-Triana M, Stecyk E, Schudoma C, Zhang W, Yang L, Miñambres M, Walther D, Schulze WX, Paz-Ares J, et al (2015) Endogenous Arabidopsis messenger RNAs transported to distant tissues. Nat Plants 1: 15025
Google Scholar: Author Only Title Only Author and Title

Towbin H, Staehelin T, Gordon J (1979) Electrophoretic transfer of proteins from polyacrylamide gels to nitrocellulose sheets: procedure and some applications. Proc Natl Acad Sci USA 76: 4350–4354
Google Scholar: Author Only Title Only Author and Title

Varotto C, Maiwald D, Pesaresi P, Jahns P, Salamini F, Leister D (2002) The metal ion transporter IRT1 is necessary for iron homeostasis and efficient photosynthesis in Arabidopsis thaliana. Plant J 31: 589–599
Google Scholar: Author Only Title Only Author and Title

Vert G, Briat J-F, Curie C (2003) Dual regulation of the Arabidopsis high-affinity root iron uptake system by local and long-distance signals. Plant Physiol 132: 796–804
Google Scholar: Author Only Title Only Author and Title

Vert G, Grotz N, Dédaldéchamp F, Gaymard F, Guerinot ML, Briat J-FF, Curie C (2002) IRT1, an Arabidopsis transporter essential for iron uptake from the soil and for plant growth. Plant Cell 14: 1223–33
Google Scholar: Author Only Title Only Author and Title

Wang H-Y, Klatte M, Jakoby M, Bäumlein H, Weisshaar B, Bauer P (2007) Iron deficiency-mediated stress regulation of four subgroup Ib BHLH genes in Arabidopsis thaliana. Planta 226: 897–908
Google Scholar: Author Only Title Only Author and Title

Warren CR (2008) Rapid measurement of chlorophylls with a microplate reader. J Plant Nutr 31: 1321–1332
Google Scholar: Author Only Title Only Author and Title

Winter D, Vinegar B, Nahal H, Ammar R, Wilson GV, Provart NJ (2007) An "Electronic Fluorescent Pictograph" browser for exploring and analyzing large-scale biological data sets. PLoS One 2: e718
Google Scholar: Author Only Title Only Author and Title

Yang T, Lin W-D, Schmidt W (2010) Transcriptional Profiling of the Arabidopsis Iron Deficiency Response Reveals Conserved Transition Metal Homeostasis Networks. Plant Phys 152: 2130–2141
Google Scholar: Author Only Title Only Author and Title

Zamioudis C, Hanson J, Pieterse CM (2014) β-Glucosidase BGLU42 is a MYB72-dependent key regulator of rhizobacteria-induced systemic resistance and modulates iron deficiency responses in Arabidopsis roots. New Phytol 204: 368–379
Google Scholar: Author Only Title Only Author and Title

Zamioudis C, Korteland J, Pelt JAV, Hamersveld M van, Dombrowski N, Bai Y, Hanson J, Verk MCV, Ling H-Q, Schulze-Lefert P, et al (2015) Rhizobacterial volatiles and photosynthesis-related signals coordinate MYB72 expression in Arabidopsis roots during onset of induced systemic resistance and iron-deficiency responses. Plant J 84: 309–22

Google Scholar: Author Only Title Only Author and Title

Zheng L, Baumann U, Reymond JL (2004) An efficient one-step site-directed and site-saturation mutagenesis protocol. Nucleic Acids Res 32, e115

Google Scholar: Author Only Title Only Author and Title

Zuo Y, Zhang F (2011) Soil and crop management strategies to prevent iron deficiency in crops. Plant Soil 339: 83–95

Google Scholar: Author Only Title Only Author and Title